AN APPLICATION OF LASER-RAMAN-SPECTROSCOPY TO THERMOCHEMICAL MEASUREMENTS IN AN ARC-HEATED WIND TUNNEL FLOW

Anthony A. Boiarski, et al

Technology, Incorporated

Prepared for:

Aerospace Research Laboratories

December 1972

ARL 72-0126
DECEMBER 1972

Aerospace Research Laboratories

AN APPLICATION OF LASER-RAMAN-SPECTROSCOPY TO THERMOCHEMICAL MEASUREMENTS IN AN ARC-HEATED WIND TUNNEL FLOW

ANTHONY A. BOIARSKI
TECHNOLOGY, INC.

FRED L. DAUM
FLUID DYNAMICS FACILITIES RESEARCH LABORATORY

CONTRACT F33615-71-C-1463
PROJECT 7065

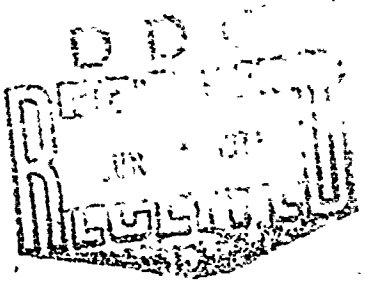

Approved for public release; distribution unlimited.

AIR FORCE SYSTEMS COMMAND
United States Air Force

NOTICES

When Government drawings, specifications, or other data are used for any purpose other than in connection with a definitely related Government procurement operation, the United States Government thereby incurs no responsibility nor any obligation whatsoever; and the fact that the Government may have formulated, furnished, or in any way supplied the said drawings, specifications, or other data, is not to be regarded by implication or otherwise as in any manner licensing the holder or any other person or corporation, or conveying any rights or permission to manufacture, use, or sell any patented invention that may in any way be related thereto.

Agencies of the Department of Defense, qualified contractors, and other Government agencies may obtain copies from:

Defense Documentation Center
Cameron Station
Alexandria, VA 22314

This document has been released (for sale to the public) to:

National Technical Information Services
Clearinghouse
Springfield, VA 22151

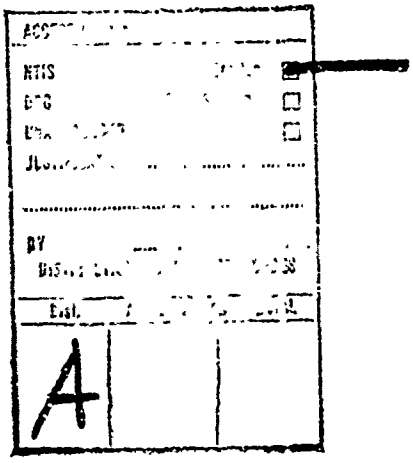

Copies of ARL Technical Reports should not be returned to the Aerospace Research Laboratories unless return is required by security considerations, contractual obligations, or notices on a specific document.

AIR FORCE/56780/21 May 1973 — 400

ARL 72-0126

AN APPLICATION OF LASER-RAMAN-SPECTROSCOPY TO THERMOCHEMICAL MEASUREMENTS IN AN ARC-HEATED WIND TUNNEL FLOW

ANTHONY A. BOIARSKI
TECHNOLOGY, INC.

FRED L. DAUM
FLUID DYNAMICS FACILITIES RESEARCH LABORATORY

DECEMBER 1972

CONTRACT F33615-71-C-1463
PROJECT NO. 7065

AEROSPACE RESEARCH LABORATORIES
AIR FORCE SYSTEMS COMMAND
UNITED STATES AIR FORCE
WRIGHT-PATTERSON AIR FORCE BASE, OHIO

FOREWORD

This report was prepared by Dr. Anthony A. Boiarski, Visiting Research Scientist, Technology, Incorporated under Contract F33615-71-C-1463 and Mr. Fred L. Daum of the Fluid Dynamics Facilities Research Laboratory, Aerospace Research Laboratories, Wright-Patterson Air Force Base, Ohio.

The authors wish to acknowledge the excellent cooperation of the professional and technical staff of the Air Force Flight Dynamics Laboratory (AFFDL) while experimental Raman scattering data were being obtained in the AFFDL 50-Megawatt Reentry Nose Tip (RENT) Facility.

UNCLASSIFIED
Security Classification

DOCUMENT CONTROL DATA - R & D

(Security classification of title, body of abstract and indexing annotation must be entered when the overall report is classified)

1. ORIGINATING ACTIVITY (Corporate author) Fluid Dynamics Facilities Research Laboratory Aerospace Research Laboratories (AFSC) Wright-Patterson AFB, Ohio 45433	2a. REPORT SECURITY CLASSIFICATION Unclassified 2b. GROUP

3. REPORT TITLE

AN APPLICATION OF LASER-RAMAN-SPECTROSCOPY TO THERMOCHEMICAL FLOW MEASUREMENTS IN AN ARC-HEATED WIND TUNNEL

4. DESCRIPTIVE NOTES (Type of report and inclusive dates)
Scientific Final

5. AUTHOR(S) (First name, middle initial, last name)

Anthony A. Boiarski
Fred L. Daum

6. REPORT DATE December 1972	7a. TOTAL NO. OF PAGES ~~80~~ 93	7b. NO. OF REFS 20
8a. CONTRACT OR GRANT NO. F33615-71-C-1463 b. PROJECT NO. 7065-03-23 c. DOD Element 61102F d. DOD Subelement 681307	9a. ORIGINATOR'S REPORT NUMBER(S) ARL 72-0126 9b. OTHER REPORT NO(S) (Any other numbers that may be assigned this report)	

10. DISTRIBUTION STATEMENT
Approved for public release; distribution unlimited.

11. SUPPLEMENTARY NOTES TECH OTHER	12. SPONSORING MILITARY ACTIVITY Aerospace Research Laboratories/LF Air Force Systems Command Wright-Patterson AFB, Ohio 45433

13. ABSTRACT

Laser Raman Scattering (LRS) has been investigated as a possible approach toward providing a nonperturbing flow calibration method for arc-heated wind tunnel facilities. Such a calibration is needed to evaluate the chemical and thermodynamic properties of the high temperature air flow which cannot be accurately determined using standard probe techniques. Theoretical calculations showed that the number densities and vibrational temperatures of nitrogen, oxygen, and nitric oxide could be obtained using the Raman spectroscopic method. Exploratory experimental LRS results obtained in the Air Force Flight Dynamics Laboratory 50-Megawatt Reentry Nose Tip (RENT) Facility showed that it is indeed feasible to apply LRS to arc-tunnel flow diagnostics.

DD FORM 1 NOV 65 1473

UNCLASSIFIED
Security Classification

14. KEY WORDS	LINK A		LINK B		LINK C	
	ROLE	WT	ROLE	WT	ROLE	WT
Raman spectroscopy						
plasma flow analysis						
flow diagnostic methods						
arc-tunnel flow analysis						

*U.S.Government Printing Office: 1973 — 759-493/519

TABLE OF CONTENTS

LIST OF ILLUSTRATIONS

NOMENCLATURE

$A(\Delta\lambda)$	apparatus function
a_o	trace scattering constant
B_e	rotational constant, cm^{-1}
B_v	rotational constant in a vibrational state, cm^{-1}
c	velocity of light, cm/sec
D_e	rotational constant, cm^{-1}
D_v	rotational constant, cm^{-1}
E	energy, joules
ΔE	quantized energy change, joules
F(J)	rotational term, cm^{-1}
G(v)	vibrational term, cm^{-1}
g_J	spin degeneracy factor
h	Plancks' constant, joule - sec
I	radiation intensity, photons/sec
J	rotational quantum number
ℓ	scattering volume length, cm
N	photon flux, sec^{-1}
N_{PE}	time rate of photoelectric events, sec^{-1}
n	number density, cm^{-3}
Q_e	photocathode quantum efficiency
S_J	rotational line strength factor
S_v	vibrational band strength factor
T	temperature, °K
T_λ	transmission coefficient
v	vibrational quantum number

α_e	rotational constant, cm^{-1}
β_e	rotational constant, cm^{-1}
$\Delta\nu$	frequency shift, cm^{-1}
ϵ	optical efficiency
λ	wavelength, Å
μ	wave number, cm^{-1}
σ	scattering cross section, cm^2/particle-sr
Ω	solid angle of collection optics, sr
ω_e	vibrational constant, cm^{-1}
$\omega_e x_e$	vibrational constant, cm^{-1}
$\omega_e y_e$	vibrational constant, cm^{-1}

Subscripts

i	incident value; integer label
o	original value
J	rotational state
p	maximum $A(\Delta\lambda)$ value; spectrometer wavelength setting
v	vibrational state
λ	wavelength
Rot, r	rotational energy mode
vib	vibrational energy mode
opt	optical property
STAND	standard

Superscripts

Q	Q-branch
S	S-branch
O	O-branch

SECTION I

INTRODUCTION

Arc-heated wind tunnels are being used in the testing associated with the development of present and future high speed flight vehicles. However, diagnostic techniques for measuring the basic flow properties in such high temperature test facilities are lacking. Therefore, development of adequate flow calibration methods is needed to provide accurate analysis of the arc-heated air plasma flow test environment which is being used to simulate free-flight conditions. For this high energy flow situation, the wind tunnel calibration should include the determination of the free stream translational, rotational, vibrational and electronic temperatures to ascertain the degree of thermodynamic equilibrium in the test gas. Also, the molecular number densities of the major, and some important minor, gas species present should be determined in order to establish the chemical state of the effluent. Further, a measure of the flow impurities such as copper electrode vapor should be obtained.

Pitot probes and heat-flux probes have been used to determine the enthalpy distribution across the test section.[1] These standard pressure and temperature probes cannot be used to determine unambiguously the free stream gas properties ahead of the bow shock wave which stands in front of the probes. Therefore, it is generally accepted that spectroscopic techniques, which do not interfere with the flow, must be employed to determine the critical thermo-chemical information. Of the various spectroscopic methods, electron beam-induced emission techniques[2,3] have been used to obtain vibrational and rotational temperatures of nitrogen and nitrogen number density in low density (generally pressures less than about two torr) arc-heated flows. Absorption, chemiluminescence continuum emission and resonance scattering methods[4,5] have also been

applied to arc-tunnel diagnostics in order to ascertain the properties of various heteronuclear molecules of interest. Finally, free-bound continuum emission[6] and copper line emission[4] techniques for determining the static temperature of the test gas have been attempted. All of the spectroscopic techniques mentioned can yield information about some properties of certain constituents in the plasma flow. However, none is generally applicable for performing a complete and accurate calibration of the more important molecular constituents of the arc-heated effluent over a wide density range. Other spectroscopic methods must be investigated to obtain the required calibration using a single measuring technique. Urtz[7] suggested that the chemical and thermodynamic state of the molecular species in a plasma could be determined by utilizing the laser Raman scattering (LRS) technique. Here, through spectroanalysis of the light scattered by plasma constituents, point measurements of important high temperature test gas parameters can be determined. Several Raman scattering experiments concerning application of this spectroscopic technique to low-temperature gasdynamic flows have been reported.[8,9] To date, however, no known attempt has been made to utilize LRS in an arc-tunnel flow analysis.

In the present report, the feasibility of using LRS in arc-tunnel flow diagnostics is investigated. Theoretical computations which demonstrate that the technique can be used to measure the rotational and vibrational temperatures and the number density of the major arc-flow constituents are presented. Experimental data which demonstrate that LRS can be applied specifically to flow calibration in the Reentry Nose Tip (RENT) arc-heated gas dynamic facility at the Air Force Flight Dynamics Laboratory, Wright-Patterson Air Force Base, are also presented. A general discussion of the Raman effect and the problems involved with making such spectroscopic measurements in arc-tunnel flows is also presented.

The present experiments in the RENT facility were exploratory in nature and were aimed primarily at determining the feasibility of such measurements. The data were obtained in a "piggyback" arrangement which limited the quantity of useful information which could be obtained throughout the investigation; the instrumentation design and installation had to be accomplished in a manner so as not to interfere with the normal test program being carried out in the RENT facility. In the preliminary study, mostly molecular nitrogen data were obtained and, therefore, this particular flow constituent is emphasized in the following text.

SECTION II

LASER RAMAN SPECTROSCOPY OF HIGH TEMPERATURE AIR

1. GENERAL DISCUSSION

In 1928, Raman[10] observed that when certain molecules were irradiated with monochromatic light of frequency ν_0 the scattered light contained not only the incident light frequency (i.e., Rayleigh scattering) but also several shifted frequencies $\nu_0-\nu_1$, $\nu_0-\nu_2$, and others. $\nu_0+\nu_1$ and $\nu_0+\nu_2$. It was noted that ν_1 and ν_2 were frequencies which were characteristic of the scattering molecule. This frequency shift phenomenon became known as the Raman effect. The radiation shifted toward lower frequencies is called "Stokes" radiation and the weaker radiation at higher frequencies "anti-Stokes." Since its discovery, the Raman scattering effect has been examined for many different molecules and has been an important tool used by physicists for studying molecular structure at known densities and temperatures. Investigators considered it an experimental method complementary to the well known absorption techniques used in previous molecular studies. Until recently, the aerodynamicist had little concern for the Raman effect because the very low scattering intensities available when using early monochromatic light sources implied excessive measurement times. Also, in the past there was little need for such a powerful diagnostic device since standard probes could analyze the thermodynamic state of a non-reacting perfect gas flow.

However, two events have altered the picture considerably. The advent of space exploration with the concomitant atmospheric reentry problems created a need for high temperature chemically-reacting flow analysis, and the development of modern high-intensity laser sources provided the Raman intensities required for on-line spectroscopic analysis. The method in which the Raman effect can be used by the aerodynamicist to analyze the

chemical and thermodynamic state of high temperature plasma flows is presented below.

2. BASIC DESCRIPTION OF THE RAMAN EFFECT

Raman phenomena can be explained by considering the molecule-photon interaction from the standpoint of conservation of energy. The incident photon at frequency $\nu_0 \text{cm}^{-1}$ and energy $E_0 = h c \nu_0$ interacts with the molecule having energy E_m. This inelastic interaction produces a scattered photon of a different energy, $E_{Raman} = h c \nu_{Raman}$, at a shifted frequency ν_{Raman}. The energy differential is accounted for through a gain or loss of energy by the molecule. Since the molecular energy is quantized, only discreet amounts of energy may be exchanged in the interaction. Hence the molecule must have an energy E_m^1 after the interaction which differs from its initial energy by a specified amount $\Delta E_{rot-vib}$. This energy differential is a known function of the bound energy states of the particular scattering molecule. The photon energies (i.e., frequencies) observed in Raman scattering must then correspond to the photon energy of the incident radiation shifted by an amount which is characteristic of the scattering molecule. The amount of frequency shift is given by

$$\nu_0 \pm \nu_{Raman} = \frac{\Delta E_{rot-vib}}{hc} \qquad (1)$$

At first there seems to be a myriad of possibilities for the scattered photon frequencies due to the many possible molecular vibrational energy states, denoted by quantum number v, each having many associated rotational energy levels, denoted by the quantum number J. However, there are selection rules which govern molecular energy transitions which can occur between various energy levels. The selection rules for a diatomic molecule undergoing Raman transitions are

$$\Delta v = 0, \pm 1 \text{ (for vibrational transitions)} \quad (2)$$

and

$$\Delta J = 0, \pm 2 \text{ (for rotational transitions)} \quad (3)$$

These selection rules limit the number of allowed frequency shifts tremendously. However, in this study even fewer transitions will be investigated since only the $\Delta v=+1$ transitions will be considered. These transitions given rise to the so-called Stokes vibrational Raman effect.

A molecular energy potential diagram and the corresponding Raman frequency spectrum is shown in Fig. 1. Only the $v=0$ to $v=1$ vibrational transition is shown, including several possible ΔJ rotational transitions. The $J=0$ to $J=0$ transition gives rise to a frequency which belongs to the Q-branch of the rotation-vibration spectrum. The $J=0$ to $J=2$ and $J=2$ to $J=0$ transitions result in S- and O-branch frequency shifts, respectively. The cross section for $\Delta J=0$ Q-branch transitions is considered to be one order of magnitude greater than those of the $\Delta J=\pm 2$ O and S satellite branches. Also, the line spacing of Q-branch lines is approximately one order of magnitude smaller than for the O- and S-branch lines. The broader line spacing of the O- and S-branches implies that few of the lines will add to the satellite branch convolution with narrow slit functions, while a large portion of the Q-branch will contribute. Hence, O- and S-branch transitions can often be omitted in the unresolved spectral intensity calculations. However, for broad apparatus functions, more satellite lines will contribute to the unresolved spectrum and their contribution cannot be neglected.

Even with the restrictions in Eqs (2) and (3), many transitions are still possible. This becomes evident, for example, when considering the Stokes Q-branch $v=0$ to $v=1$ vibrational transition, where the $J=1$ to $J=1$, $J=2$ to $J=2$, etc. rotational transitions can occur as well as the $J=0$ to $J=0$

transition shown in Fig. 1. Due to small differences in rotational energy level spacing, the resulting frequencies are quite close but distinguishable. Also, v=1 to v=2, v=2 to v=3, etc. vibrational transitions can occur with all the $\Delta J=0$ transitions included in each $\Delta v=1$ vibrational transition. The various vibrational transitions are easily distinguished due to molecular anharmonicity. Hence, 1000-2000 Raman Q-branch transitions may be considered in the analysis of the Stokes rotation-vibration spectrum. Inclusion of $\Delta J=\pm 2$ transitions increases the number threefold.

The nomenclature used in this text to identify Raman transitions and spectral features will be as follows:

a. Various branches will be identified by their specific transition $v_1 \rightarrow v_2$ as (v_1,v_2). Hence, the v=0 to v=1 Q-branch transitions are identified as the (0,1) Q-branch.

b. Within a specific branch the rotational lines are identified by the rotational quantum number of the initial state involved in the transition. For example, the J=2 to J=0 transition is labeled O-branch J=2 rotational line.

c. Branches are sometimes referred to as vibrational bands.

3. ROTATION-VIBRATION LINE INTENSITIES

Smekal[11] predicted the Raman effect in 1923 and since that time the theory of Raman scattering has become well developed from both the quantum mechanical and the semi-classical viewpoints.[12,13] Hence, only the results of the detailed theoretical investigations will be presented in this report.

The total number of observed Raman photons/second, resulting from a particular Stokes rotation-vibration transition is given by

$$N_{v,J} = N_i \chi_{v,J} \sigma_{v,J} \Omega \ell n \qquad (4)$$

where N_i is the number of incident photons/second, ℓ is the optically observed length of the laser beam in centimeters, Ω is

the solid angle of the collection optics in steradians, n is the number of molecules per cubic cm in the gas sample and $\chi_{v,J}$ is related to the fraction of molecules in energy state $E_{v,J}$. The symbol $\sigma_{v,J}$ is the scattering cross section (i.e., cm^2/particle-sr) or transition probability for the particular $v \rightarrow v+1$, $J \rightarrow J$, $J\pm2$ transition and is written as

$$\sigma_{v,J} = K(\nu_0-\Delta\nu_{v,J})^4 g_J S_v \tag{5}$$

where K is a constant which can be theoretically estimated and experimentally measured. The frequency shift $\Delta\nu_{v,J}$ of the Raman line is given by[14]

$$\Delta\nu^Q_{v,J} = \Delta\nu_v-\alpha_e J(J+1)-\beta_e J^2(J+1)^2$$

where $J = 0,1,2,\cdots$ for Q-branch lines,

$$\begin{aligned}\Delta\nu^O_{v,J} = {} & \Delta\nu_v-\left[D_{v+1}-D_v\right]J^4+\left[6D_{v+1}+2D_v\right]J^3 \\ & +\left[B_{v+1}-B_v-13D_{v+1}+D_v\right]J^2 \\ & -\left[3B_{v+1}+B_v-12D_{v+1}\right]J+2B_{v+1}-4D_{v+1}\end{aligned} \tag{6}$$

where $J = 2,3,4,\cdots$ for O-branch satellite lines,

$$\begin{aligned}\Delta\nu^S_{v,J} = {} & \Delta\nu_v-\left[D_{v+1}-D_v\right]J^4-\left[10D_{v+1}-2D_v\right]J^3 \\ & +\left[B_{v+1}-B_v-37D_{v+1}+D_v\right]J^2 \\ & +\left[5B_{v+1}-B_v-60D_{v+1}\right]J+6B_{v+1}-36D_{v+1}\end{aligned}$$

where $J = 0,1,2,\cdots$ for S-branch lines, and

$$\Delta\nu_v = \omega_e-2\omega_e x_e(v+1)+\omega_e y_e(3v^2+6v+13/4)$$

The rotation-vibration coupling constants B_v, B_{v+1}, D_v, D_{v+1} in Eq (6) are written as

$$B_k = B_e - \alpha_e(k+1/2)$$

$$D_k = D_e + \beta_e(k+1/2) \tag{7}$$

In Eqs (6) and (7) above, ω_e, $\omega_e x_e$ and $\omega_e y_e$ are vibrational constants and α_e, β_e, B_e and D_e are rotational constants of the scattering molecule. The values of the above parameters used in the calculations reported in this text were taken from Ref 14. The symbol g_J in Eq (5) is the spin degeneracy factor, which depends on whether J is an even or odd integer, and S_v, the vibrational band-strength factor, is given by

$$S_v = v+1 \tag{8}$$

From Eq (8), it can be seen that a v=1 to v=2 transition has a probability of occurring twice that of the v=0 to v=1. For a Boltzmann population distribution $X_{v,J}$ is a function of the vibrational temperature T_v and the rotational temperature T_r of the scattering molecule and is written

$$X_{v,J} = \frac{S_J e^{-\frac{1.44F(J)}{T_r}} e^{-\frac{1.44G(v)}{T_v}}}{Q_{rot}\, Q_{vib}}$$

where the state sums Q_{rot} and Q_{vib} are given as

$$Q_{rot} = \sum_J (2J+1) e^{-\frac{1.44F(J)}{T_r}} \tag{9}$$

$$Q_{vib} = \sum_v e^{-\frac{1.44G(v)}{T_v}}$$

The functions F(J) and G(v) which appear in Eq (9) are written as

$$F(J) = B_v J(J+1) - D_v J^2 (J+1)^2$$

and (10)

$$G(v) = \omega_e (v+1/2) - \omega_e x_e (v+1/2)^2 + \omega_e y_e (v+1/2)^3$$

In Eq (9) S_J is the line strength factor, which is given by

$$S_J^Q = a_0(2J+1) + \frac{J(J+1)(2J+1)}{(2J-1)(2J+3)}, \quad J=0,1,2\cdots$$

for the Q-branch, and

$$S_J^O = \frac{3(J-1)J}{2(2J-1)}, \quad J=2,3,4\cdots \qquad (11)$$

for the O-branch, and

$$S_J^S = \frac{3(J+1)(J+2)}{2(2J+3)}, \quad J=0,1,2\cdots$$

for the S-branch.

In Eq (11), a_0 is the so-called trace-scattering constant, which was assumed to have a value of 4.0 in the computations discussed next.

Using the above equations, the temperature dependence of the Q-branch Raman rotation-vibrational lines of molecular nitrogen was calculated for illustrative purposes. The results for the even rotational lines at $T_v = T_r = 300°K$ and $1000°K$ are plotted in Fig. 2. The shift in the rotational intensity peak within a given rotation-vibration band as the temperature increases is noted. This so-called "blue shift" is due to the increase in population of the upper rotational states with increasing rotation temperature. Also, the appearance at about 3654 Å of the (1,2) Q-branch at 1000°K is evident. These upper

state Raman transitions appear in the spectrum due to the increase in the population of the upper vibrational states with increasing vibrational temperature.

The above equations and calculations show that the Raman line intensities are functions of number density, rotational temperature, vibrational temperature and various molecular constants. Further, Raman frequency shifts are uniquely dependent on the scattering molecule. Hence, a measurement of the frequency spectrum can yield an identification of the molecules which are present in the test sample. Also, the concentration of each constituent and the rotational and vibrational temperatures of each molecular species can be determined from a spectral intensity analysis.

4. COMPUTATION OF THEORETICAL RAMAN SPECTRA

In practice, a spectrum such as that shown in Fig. 2 would be difficult to obtain due to the high resolution required to give individual line intensities and due to the overlap of rotational lines of adjacent Q-branches. Hence, unresolved spectra will normally be obtained experimentally. To compute the unresolved spectral intensity, the Raman line intensities given above must be convoluted with the apparatus function of the measuring instrument. The apparatus function, with a peak transmission λ_p, may be scanned through the spectrum. The unresolved spectral intensity N_{λ_p} at wavelengths λ_p is given by

$$N_{\lambda_p} = \sum_{v,J} N_{v,J}\, A(\Delta\lambda)$$

and

$$\Delta\lambda = \lambda_p - \lambda_{v,J} \qquad (12)$$

where

$$\lambda_{v,J} = \frac{10^8}{\nu_0 - \Delta\nu_{v,J}}$$

Here, $A(\Delta\lambda)$ is the apparatus function and $N_{v,J}$ and $\Delta\nu_{v,J}$ are the Raman line intensities and frequency shifts, respectively, given by the detailed equations in the previous section. By varying λ_p through the region of the Raman lines, the unresolved spectral scan can be determined theoretically using a digital computer program to perform the straightforward but tedious computations. An example of such a calculation for molecular nitrogen at a constant number density and temperatures of 300°K and 3000°K is shown in Fig. 3. A 1 Å-wide trapezoidal apparatus function was assumed, and only Q-branch transitions were included in the computations. Note that individual rotational lines are not detectable since the apparatus function is wide enough to include many lines at once. However, the various Q-branches are able to be resolved with this particular apparatus function. Also, note the vast difference in the spectra at the two temperatures shown in Fig. 3. At 300°K the Raman spectrum is limited to a narrow region of the total spectrum while at 3000°K a much broader wavelength interval is covered.

Since most early Raman work was done at room temperature or below, the term Raman "line" was adopted, since the Raman spectrum looked like a "line" (e.g., see Fig. 3). However, approximately 20 actual rotational lines make up the Q-branch spectrum at room temperature, as shown in Fig. 2, and, therefore, the term "line" is incorrect. At higher temperatures, where other Q-branches appear due to upper level vibrational transitions, the term "line" becomes meaningless as well as incorrect. Therefore, a better term would be Raman "rotation-vibration spectrum" or just "Raman spectrum," which has been adopted in this text. Even more specifically, at 300°K the prominent Raman spectrum would be correctly referred to by calling it the Raman "(0,1) Q-branch."

The apparatus function used in the calculation plotted in Fig. 3 was quite narrow for the spectral analyzer used in this study. Therefore, a more realistic triangular apparatus function

having a half-width of 23 Å was used to compute the unresolved Raman spectrum. A plot of these results is shown in Fig. 4 for various nitrogen temperatures and for thermodynamic equilibrium conditions (i.e., $T=T_r=T_v$). Only $\Delta J=0$ transitions were used in the computations. Note that the various Q-branches are not resolved for this relatively broad apparatus function, yet the spectral intensity profile is quite sensitive to gas temperatures above 1000°K.

5. DETERMINATION OF CHEMICAL AND THERMODYNAMIC STATE OF AIR

a. Rotational Temperature

For a particular $\Delta v=1$ transition (i.e., (0,1) Q-branch), Eq (4) can be written

$$\frac{N^Q_{0,J}}{N_{0,0}} = \left[\frac{(\nu_0-\Delta\nu_{0,J})}{(\nu_0-\Delta\nu_{0,0})}\right]^4 \frac{S_J g_J}{S_0 g_0} e^{-\frac{1.44F(J)}{T_r}} \qquad (13)$$

Thus, the relative line intensity distribution in a given Q-branch is a function only of the rotational temperature of the gas. This can be readily observed in Figs. 2 and 3, where the wavelength of peak intensity in the (0,1) Q-branch has shifted toward the blue end of the spectrum at the higher temperature condition. Also, note that the asymmetry of the spectral profile is quite different for the elevated temperature case. Thus, by curve fitting the spectral profile of the (0,1) Q-branch and/or any other branch, the rotational temperature of the gas can be obtained from the rotation-vibration spectrum. Since the branches must be resolved, the narrower apparatus function, such as that used in Fig. 3, must be used in order to obtain information on the rotational state of the scattering molecules.

b. Vibrational Temperature

Summing Eq (4) over the rotational quantum number J will result in the following expression

$$\left(\frac{N_v}{N_0}\right)^Q = \left(\frac{\nu_0-\Delta\nu_v}{\nu_0-\Delta\nu_0}\right)^4 S_v e^{-\frac{1.44G(v)}{T_v}} \qquad (14)$$

where

$$\Delta\nu_v = \omega_e - 2\omega_e x_e(v+1) + \omega_e y_e(3v^2+6v+13/4) \qquad (15)$$

Hence, the relative integrated intensity of the Q-branch is indicative of the vibrational state of the gas. In other words, the shape of each branch is a function of the rotational temperature, but the relative intensity of the various branches is dependent only on the vibrational temperature of the scattering molecules. It must be pointed out that, in general, accurate integrated Q-branch intensities are difficult to obtain due to the overlap of the various branches. Thus, Eq (14) cannot be used in most cases to calculate the vibrational temperature from the unresolved spectrum. Instead, curve fitting techniques must be employed to obtain the vibrational temperature of the gas. Note that both of the above spectral analysis methods require only relative intensity measurements; no absolute intensities are needed.

For equilibrium conditions (i.e., $T_v=T_r=T$), a curve fit of the entire spectral intensity profile can be used to obtain the gas temperature. Either narrow or broad apparatus functions can be used. However, if thermodynamic nonequilibrium is suspected, a separate curve fit must be made of one or more Q-branches to determine the rotational temperatures independently of the vibrational state of the gas. Then, the vibrational temperature can be determined from a curve fit of the entire rotation-vibration spectrum. The rotational temperature of the gas can be used as data for this calculation. Note, that

narrow apparatus functions must be used for the nonequilibrium case in order to determine independently the rotational and vibrational states of the test gas.

c. Number Density

A cursory examination of Eq (4) might imply that the Raman spectrum could be used directly to evaluate the number density of a gas under varying temperature conditions. This is not true since Raman line intensities are dependent upon temperature and number densities simultaneously. This coupling of number densities and temperature is common to all spectroscopic techniques and arises from temperature effects on the population distribution of the various energy modes. The coupling effect can be readily demonstrated by considering the spectral plot shown in Fig. 3, where constant number density was assumed in the calculations. Note that if the (0,1) Q-branch peak intensity were to be used to compute number density at 3000°K without making correction for temperature effects, the calculated values, compared to room conditions, would be in error by a factor of 3. Hence, the gas temperature must be known in order to obtain the correct number density of any of the species in the test gas. For nonequilibrium conditions, the temperatures of the vibrational and rotational modes must be obtained in order to correct for temperature dependence. The temperature effects on number density measurement can be minimized under certain circumstances. Note that by using a broader apparatus function, as shown in Fig. 4, the resulting nitrogen Raman spectrum is nearly temperature independent at 3663 Å. Hence, by choosing proper experimental conditions the need for temperature corrections can be eliminated if a certain amount of calculable error is tolerable. In this case, the intensity of the nitrogen Raman spectrum at 3663 Å is nearly directly proportional to the number density of nitrogen for the particular apparatus function used in the calculations. Varying the shape of the apparatus function will change the optimum wavelength and also the error estimates.

To determine the number density of the constituents of high temperature air, the measurement of absolute spectral intensities is not required. Those difficult absolute measurements may be avoided through the application of a calibration point which is the known composition and number density of room air existing before and/or after the high temperature test condition. Also, the number density of any species which is present only in the test environment can be determined by ratioing its intensity value to a room temperature constituent such as nitrogen. This is an attractive feature of the Raman scattering diagnostic method over other spectroscopic techniques which require either absolute intensity measurements or complex calibration procedures.

d. Consideration of Exploratory Measurements in RENT

Thermodynamic equilibrium was expected in the RENT Facility due to the high number density and static temperature of the gas. Hence, a broad apparatus function could be employed to provide spectral profiles similar to those shown in Fig. 4. These profiles could then be analyzed to determine the static temperature and species concentrations of the gases in the arc-heated flow environment. However, due to time limitations, the entire intensity vs wavelength spectrum could not be obtained. Therefore, a two-intensity technique was adopted instead. Figure 4 shows the two wavelength possibilities (3645 Å and 3663 Å) in the Raman spectrum of nitrogen for the particular triangular apparatus function used. Note that the intensity at 3645 Å is quite sensitive to the gas temperature, above 1000°K. As mentioned above, the intensity of the Raman spectrum at 3663 Å is nearly independent of temperature and is so assumed. Various ratios of these two intensities are plotted in Fig. 5. Above 1000°K, the I(3645 Å) to I(3663 Å) ratio can be used to determine the gas temperature to an accuracy approximately equal to the accuracy obtained in the intensity ratio measurement.

Figure 5 also verifies that the intensity at 3663 Å can be used to measure nitrogen number density directly without correcting for temperature. Hence,

$$n_{N_2} = \frac{I(3663\text{Å})_T}{I(3653\text{Å})_{300}} \left(n_{N_2}\right)_{STAND} \tag{16}$$

The above equation holds to within an acceptable error throughout the temperature range of interest. In Eq (16) n_{N_2} and $(n_{N_2})_{STAND}$ are the unknown and standard number densities of nitrogen in particles/cm^3. The value of $I(3663\ \text{Å})_{300}$ is obtained from a pre- and post-run calibration using room temperature air as mentioned above. The number density and temperature of other gases could be obtained in a similar manner.

Figure 6 shows a digital computer calculation of the entire Stokes Raman rotation-vibration spectrum of air at room temperature and at the density conditions expected in the arc-tunnel test flow. These computations were performed for the actual apparatus function of a Jarrell-Ash 1/4-meter spectrometer having 500-μm slits. Note that the spectra of the various gases are quite distinct and only slightly overlapped. Evaluation of the tunnel spectral data using the above methods will, therefore, yield the thermodynamic and chemical state of the major constituents in the arc-heated plasma.

SECTION III

THE ARC-TUNNEL ENVIRONMENT

1. GENERAL DISCUSSION OF MEASUREMENT PROBLEMS

Flow diagnostics in the arc-tunnel environment present many serious experimental difficulties for the spectroscopist and aerodynamicist. Hence, relatively little has been learned about these high temperature chemically reacting flows. Furthermore, each test facility is somewhat unique and every effort to overcome the specific individual problems and make flow measurements in these facilities is important. In the following text, the general problems will be discussed and possible solutions suggested.

Several experimental difficulties are common to all arc-tunnel flow environments, while others are unique to the particular facility. The degree to which each may hinder spectroscopic measurements differs from case to case. The arc which is used to heat the test gas requires high electrical currents and voltages. Fluctuations in these quantities induce electrostatic and magnetic fields which can affect electronic instruments and electric signals. Also, these fields may critically affect the photomultiplier tubes used in spectroscopic data acquisition. Hence, the electrical environment of all arc tunnels can hinder spectral measurements. To minimize these possible induced field effects, electrostatic and magnetic shielding of electronic instruments should be used, especially if they are in close proximity to the arc. Also, double shielded signal cables will reduce some of these unwanted effects. Finally, a mu-metal shield for the photomultiplier tube is recommended.

The high effluent and electrode temperatures, which are common to arc tunnels, also create several possible light absorption problems. The chemical constituents of high temperature air include nitrogen dioxide NO_2, and NO, nitric

oxide. Also, the large amounts of water cooling required for the electrodes present the possibility of water vapor, H_2O, contamination of the flow due to leaks or residual amounts from previous heater failures. These heteronuclear molecules will absorb in various regions of the spectrum. This absorption can interfere with spectroscopic measurements and little can be done about this except to try to avoid working in those regions of the spectrum where flow absorption is a problem. Of course, absorption spectroscopy is itself a technique which can be applied to gas analysis of heteronuclear molecules such as NO. For a discussion of some of the difficulties in making absorption measurements in arc-tunnel flows, the reader should consult Ref 4. Due to errosion and evaporation of the electrodes in arc-heated facilities, metal particle and metal vapor absorption can also occur. This type of absorption is broad-banded (i.e., it covers a large portion of the spectrum), so nothing can be done to avoid it. If absorption is not negligible, the spectroscopic data must be corrected to account for this adverse effect. It is possible for electrode material absorption and/or molecular absorption to nearly obscure the spectral data sought; therefore, the experiment should be designed to minimize and/or correct for possible absorption.

Due to the critical arc-heater cooling requirements and high electrical power consumption, run times may be quite short in typical arc-tunnel facilities. This presents a practical problem of obtaining the desired spectral intensity versus wavelength scans if the photoelectric signal is weak and some time must be spent gathering data at any given wavelength. Instrumentation which is extremely sensitive and can count the photons per second in the light signal is presently available and will be discussed later; however, the time required to make spectral scan measurements is excessive. Some new experimental instrumentation advances which allow spectral data to be obtained in much shorter times are beginning to appear on the market

and others are in the development stage. Hence, the data acquisition problem of some arc-heated facilities may be solved soon.

Another problem inherent in some arc facilities is acoustic noise and its corresponding deleterious vibration effects on experimental apparatus. The vibration of the optical components as well as electronic instruments can present serious problems to the spectroscopist. Acoustical insulation and vibration mounting must be employed in the design of the spectroscopic measuring device if acoustic noise is a problem.

2. FLOW RADIATION

One of the most difficult problems in arc-flow diagnostics is that of electromagnetic radiation coming from the hot flow. This emission can obscure the spectral signal of interest, especially if the signal is relatively weak. For example, the strong radiation from the test jet flow of the WPAFB Flight Dynamics Laboratory 50-Megawatt RENT Facility is clearly evident in the photograph presented in Fig. 7. Details of the flow emission spectra from various sources which are present in this and other arc-heated facilities are presented below.

One source of flow radiation is chemiluminescence which comes from the chemical reaction of NO with O to form NO_2. An excited molecular complex is assumed to be created in the reaction process which results in a continuum radiation being emitted during the completion of the reaction. A plot of radiation intensity versus wavelength which was obtained by Mastrup[4] is shown in Fig. 8. This continuum flow emission covers a wide range of the spectrum, from blue to near-infrared, and is, therefore, difficult to avoid. Also plotted in Fig. 8 are the laser exciting line and Raman Stokes and anti-Stokes spectral regions for the nitrogen, argon and ruby laser sources (represented by the horizontal lines). It is seen that the choice of the ultraviolet pulsed nitrogen laser for LRS

application would completely avoid the chemiluminescence problem. However, Raman scattering experiments utilizing the ruby and argon ion laser would have to contend with this background flow radiation. Other sources of unwanted radiation from the arc-heated effluent are the NO band radiation at wavelengths less than 3000 Å and the scattering of arc-radiation by electrode material in the flow. The scattered light originates in the stagnation region and passes through the nozzle throat. This so-called "flashlight effect" extends from about 3200 Å to the near infrared and consists of molecular band radiation, free-free and free-bound continuum radiation and atomic line emissions. The particle scattered radiation of the "flashlight" effect cannot be avoided through the choice of laser so it must be overcome by some other approach, if it is not negligible. Another important source of background radiation comes from spontaneous emission by excited atoms of copper and silver electrode material which are present as an impurity in the flow. Estimates of the relative intensity of various copper emission lines[4] and a silver doublet are shown in Fig. 9. The strongest lines are located near 3200 Å and 5000 Å. The 3200 Å doublet are copper resonance lines. The nitrogen, argon and ruby laser exciting wavelengths and Raman regions are also plotted in Fig. 9. Note that only the ruby Stokes region is overlapped by strong copper lines. Since these emissions result from atomic transitions, they occupy narrow regions of the spectrum and are usually not difficult to avoid. However, several exceptions exist. The resonance lines can be pressure broadened, which will widen their spectral region of influence. Also, intense radiation from these lines, or any other source for that matter, can show up as scattered light inside the spectroscopic measuring equipment, thus presenting a problem.

The pressure and temperature environment, as well as the arc power of each arc-tunnel, will dictate which of the above

radiation sources will dominate the emission spectrum of a particular facility. Thus, a prerequisite to obtaining particular spectroscopic data should be an investigation of the flow emission spectrum. In the case of Raman spectroscopy the choice of a laser source can be made so as to avoid the worst background noise problem areas. Chopped CW or pulsed lasers of narrow pulse half-width should be used in conjunction with lock-in or gating techniques in order to recover the signal from flow background emission. In other words, experimental ingenuity must be used to solve flow radiation problems.

SECTION IV

EXPERIMENTAL TECHNIQUES IN ARC-TUNNEL DIAGNOSTICS

1. GENERAL DISCUSSION

The present experimental studies were conducted in the Air Force Flight Dynamics Laboratory Reentry Nose Tip (RENT) Arc-Heated Wind Tunnel at Wright-Patterson Air Force Base. The facility consists of a high pressure, high power arc-heater; settling chamber; convergent-divergent nozzle; ambient atmosphere boundary, free jet, test region; flow collector device; and a gas cooling and scrubbing system. The arc-heater operates at 100-atmospheres pressure, heating up to 8 lbm/sec of air to stagnation enthalpies near 6000 BTU/lbm. This requires the use of electrical power approaching 37 megawatts. The air plasma is expanded from a 0.900-inch throat to Mach 1.8 at the 1.1-inch nozzle exit. Equilibrium flow calculations show that the number density of the nitrogen at the exit is approximately equivalent to that of room air; the nozzle exit pressure is about 18 atmospheres and the static temperature calculated to be near 3600°K. By adjusting the swirl of the air into the heater, either a peaked or flat enthalpy profile across the test jet can be obtained. The ratio between the centerline and intermediate plateaus of the heating rate is approximately 2:1 for the peaked profile case.

Since the RENT nozzle exhausts into the ambient atmosphere, acoustic noise and its inherent induced vibrations were a particular problem. Sound levels near 110 db were recorded with a microphone located near the nozzle exhaust. Also, the entire facility is located inside the converging nozzle entrance section of the old Flight Dynamics Laboratory 10-Foot Transonic Wind Tunnel, so non-acoustic mechanical vibration was also present. Further, the size and structure of the room which houses the RENT facility, along with the auxiliary arc heater equipment in the room, seriously limited the space available for

optical diagnostic instrumentation purposes. Also, because of the non-interference "piggyback" nature of the present Raman gas diagnostic experiments, the instrumentation configuration developed as a matter of necessity rather than optimum design. An overall view of the facility is shown in Fig. 10, where the light paths from the laser to the test section and from the test section to the spectrometer are indicated. Further details concerning the operating conditions of the arc-heater can be found in Ref 15.

2. RAMAN SCATTERING SYSTEM DESIGN

The laser Raman scattering instrumentation has several basic components (see Fig. 11). A monochromatic laser source is the heart of the system. An optical focusing system is needed to transfer and focus the laser beam into a specific test area. A means to monitor the laser power and determine if any of the laser beam is absorbed by the test gas is also needed, especially in arc-tunnel work. Receiver optics are required to collect the Raman scattered photons and focus them onto the slit of the spectral analyzer. The scattering volume observed is located at the intersection of the optical path of the receiver optics and the focused beam. The scattering volume dimensions are determined by the cross sectional area of the focused beam and the length of the focused beam covered by the receiver optics. This region defines the volume of gas which is to be analyzed by the Raman diagnostic technique.

An analyzer, usually a monochromator, is needed to determine the spectral intensity and wavelength composition of the Raman scattered photons. Finally, a photomultiplier tube and its associated electronic equipment are necessary to convert the Raman light intensities into usable electrical signals which can be processed and recorded. In arc-tunnel experiments, as stressed earlier, some means must also be devised to reduce the effect of the large amount of undesired flow radiation which is also collected by the receiver optics.

The choice of particular components for an LRS system is based upon selecting the proper experimental parameters, found in the following general Raman scattering equation (i.e., a form of Eq (4)) for obtaining a usable signal

$$N_{PE} = N_i \sigma n \Omega \ell Q_e \epsilon_{opt} T_{\lambda_{ex}} T_{\lambda_{Ram}} \tag{17}$$

where

N_{PE} = rate of Raman photoelectrons being detected, sec^{-1}

N_i = rate of incident laser photons, sec^{-1}

n = number density of scattering particles, cm^{-3}

σ = total Raman scattering cross section, $cm^2 sr^{-1}$ per particle

ℓ = scattering volume length, cm

Ω = solid angle of receiver optics, sr

Q_e = photomultiplier tube quantum efficiency

ϵ_{opt} = total optical system efficiency

$T_{\lambda_{ex}}$ = plasma transmission factor at the laser wavelength

$T_{\lambda_{Ram}}$ = plasma transmission factor at the Raman scattered wavelength

As the above equation suggests, a photon counting system was the measurement technique used in this study since it provides the maximum sensitivity in low light level applications. Each term in the above equation will be further defined in the following discussion of the system components.

a. Laser Selection

There are a number of direct and several indirect factors which enter into the selection of the laser to be used. A large average laser power, which implies a large incident photon flux N_i, is directly required in order to maximize N_{PE},

the detected flux. Also, the laser wavelength should be chosen so as to avoid any large absorption factors. However, indirectly, the laser choice influences the scattering cross section and the photomultiplier quantum efficiency due to the wavelength dependence of these parameters. The cross section σ varies as the fourth power of exciting frequency, and, therefore, blue laser light will be scattered more readily than red. Also, the highest quantum efficiencies available in contemporary photomultiplier tubes are in the blue region of the spectrum.

Another subtle effect of the laser choice is that due to the polarization properties of the laser source which result in angular variations in scattering intensity for different planes of polarization. For 90° scattering, which was used in the present study, only one component of unpolarized light is most useful in producing Raman scattering; i.e., that component which is perpendicular to the plane of observation. Hence, approximately one-half of an unpolarized laser photon flux is useless in producing detectable Raman photons for 90° scattering.

Finally, the laser beam quality, which does not appear directly in Eq (17), has an important bearing on the laser choice. Beam quality here refers to the capability of focusing the beam into a very small cross-sectional area. This criterion enters into the formulation because Eq (17) tacitly assumes that laser photons which are scattered and then collected by the optics are all focused into the spectrometer slit. However, if the image of the laser scattering volume width on the slit is larger than the slit itself due to poor beam quality, signal intensity losses will occur. Further, widening the slit to accommodate the laser beam width is sometimes not possible due to restraints on spectral resolution.

For arc-tunnel diagnostics utilizing LRS, several other criteria also should be considered. Pulsed lasers having nonosecond pulse widths, when coupled with electronic gating

techniques, can provide a means to reduce greatly the flow radiation since

$$\text{Noise Reduction} = \frac{\text{Time Between Laser Pulses}}{\text{Laser Pulse Width}} \tag{18}$$

Reduction factors of 10^6 and greater are attainable through the use of a number of commercially available lasers. Hence, the optimum laser source for the present arc-tunnel diagnostics would be a high powered blue, pulsed laser having monochromatic emission which is polarized and having a focused beam diameter which is nearly diffraction limited.

b. Focus and Collection Optics

The focusing and collection optics enter directly into Eq (17) through ϵ_{opt}, the total optical efficiency. The efficiency of each optical component should be as near to 1.0 as possible to avoid cumulative effects since

$$\epsilon_{opt} = \prod_i \epsilon_i \tag{19}$$

where ϵ_i is the efficiency of any single optical component. Hence, material choices and coatings should be selected to maximize the efficiency at the laser or Raman wavelengths, depending upon the particular use of the optical item. The performance of the collection optics enters directly into the photoelectron flux calculations through the collection solid angle Ω, which is measured in steradians and defined as

$$\Omega = \frac{\pi}{4}\left(\frac{D}{R}\right)^2 \tag{20}$$

where R is the distance of the collector lens of diameter D from a point source of light. Equation (20) is approximately correct when $R > 2D$. The optical f/-number f/No of a lens is defined as

$$f/No = \frac{\text{focal length}}{\text{diameter}} = \frac{R}{D} \tag{21}$$

Substituting in Eq (20) gives

$$\Omega = \frac{\pi}{4} \frac{1}{(f/No)^2} \tag{22}$$

Hence, the collection optics f/No is an important design parameter in the Raman experimental setup since the measured photoelectron flux varies inversely as the square of this quantity.

The focusing and image forming capabilities of the optical receiver system are indirectly coupled into Eq (17) since the scattered light must be imaged through the slit as mentioned above in the discussion of laser beam quality. Hence, poor beam quality can be partially overcome by good receiver focusing and optical reduction in the scattering volume size. This optical reduction will decrease the f/No somewhat if a bigger lens is not used to compensate for the larger distance from the scattering region. Finally, polarization effects must be considered here since certain optical components are polarization sensitive under particular experimental conditions.

c Laser Power Monitor

The laser power is monitored to provide several important parameters in the flux equation. The number of incident photons N_i must be known to compute N_{PE}. Also during an arc-tunnel test, any change in laser power between the time of calibration and the time of the measurement must be determined to correct the spectral intensity measurements for power drift effects. Besides drifts in laser power, absorption of laser and Raman photons by the flow must be evaluated in order to correct for the absorption effects given by $T_{\lambda_{ex}}$ and $T_{\lambda_{Ram}}$ in Eq (17).

The methods used to measure laser power during an arc-tunnel test can vary tremendously, but several features will be common to most experimental setups. Some photoelectric device must be used to convert the laser photon flux into an electrical signal. An analog output from the associated electronics of this component must be obtained in a time coincident with the spectral intensity measurements. Several precautions should be taken in the experimental design and use of this item. For example, saturation of the photoelectric device may be checked by measuring the output linearity of the monitoring system against changes in input light intensity. Also, the plasma flow radiation again enters into consideration since this background radiation will also be detected by the power monitoring photo-electric device. Suitable narrow band pass filters which reject all but the laser line wavelength may be employed. Also, gating techniques may be required if filtering does not adequately reduce the undesired flow emission signal.

d. Spectrometer and Associated Filtering

The spectral analyzer (i.e., spectrometer) must be able to obtain Raman intensity versus wavelength measurements. In this study it is required to perform this spectral analysis under the usual conditions of interference from Rayleigh scattered light at the laser frequency and flow background radiation which also enters the spectrometer slit and reflects around the inside of the instrument. Further, since the f/No of the receiver optical system is dependent upon the f/No's of the various components, the spectrometer f/No should be as small as practicable for Raman work. To meet these particular requirements special Raman spectrometers have been commercially produced. Some incorporate tandem single spectrometers (i.e., double spectrometers) to prevent internally reflected light at other than Raman wavelengths from reaching the photo-multiplier tube and masking the weak Raman signal. Also, most Raman spectrometers have large optical components in order to obtain small instrument f/-numbers.

The choice of spectrometer depends upon the particular Raman application. The instrument spectral bandpass (i.e., apparatus function half-width) is directly proportional to the physical slit width. If the slit width choice is dependent upon laser beam quality, focus and/or imaging optics, as mentioned above, then the spectrometer choice and utilization may be altered to obtain the proper apparatus function. That is, the instrument focal length, grating size and number of grooves per millimeter, as well as the spectral order can be picked to provide the proper bandpass at moderately large slit widths.

The choice of spectrometer enters directly into the measured photoelectron flux calculations of Eq (17) through ϵ_{opt} since the instrument transmission has a wavelength dependency. A choice of grating blaze angle to coincide with the proper spectral order to be used will maximize the instrument efficiency in the Raman region of the spectrum. Again, polarization effects must be considered since a significant difference in intensity, depending upon the orientation of the plane of polarization with respect to the surfaces of the optical components and grating grooves in the instrument, can be obtained.

It was tacitly assumed that the optical f/No remains constant across the length of the beam which is observed by the optics and spectrometer combination. The length is chosen, of course, by altering the spectrometer slit heights, which parallel the beam length image; preferably the solid angle of the light entering the slit should match the angle of the light from the slit to the collimating mirror. Also, since vignetting losses can occur if large beam lengths are observed, the optical design must be checked so that the on-axis f/No is preserved for finite beam length images.[16] These off-axis light losses effectively reduce the true length of the observed beam.

Spectral filters can be used in conjunction with spectrometers to assist in removing the unwanted internally reflected light. This can be accomplished by absorbing or otherwise interfering with the wavelengths other than those in the Raman region of the spectrum to keep them from entering the spectrometer and/or by similarly blocking the light at the photomultiplier tube. The latter is sometimes better since unwanted fluorescence can occur in filtering devices which are exposed to large light fluxes. Hence, careful choice of a spectrometer and associated collection optics, filtering components, and experimental geometry may further optimize the Raman scattering system.

e. Photomultiplier Tube

The choice of a photomultiplier tube (PMT) is somewhat related to the laser choice, since the quantum efficiency Q_e which appears in Eq (17) is highly sensitive to wavelength and the PMT cathode material. Another important criterion in PMT choice is the response time of the tube. This is usually no problem for the tube itself, but care must be taken so that the tube circuit design does not limit the overall response time since photon counting at high photon fluxes requires very short PMT response time. Also, the PMT operation at high gain, which is necessary for many photon counting applications, tube saturation must be avoided. Finally, PMT's are somewhat polarization dependent, so this fact should also be considered. Hence, judicious choice of a PMT and tube circuit design for a particular laser selection will maximize photoelectron flux measurement sensitivity and tend to optimize the performance capability of the instrument system.

f. Electronics - Single Photoelectron Counting

The electronic system for making Raman scattering measurements in arc-tunnel environments must be designed with the specific intention of measuring weak Raman radiation in the presence of the very strong flow background emission. To

accomplish this, the electronic instruments must be capable of being gated to the half-width of the laser pulse, which is typically in the 10-nanosecond time range. Also the system must be capable of accommodating and measuring Raman photoelectric events of perhaps 50 Hz or less among as many as 10^7 photoelectrons per second produced by continuous radiation from flow emission. A system capable of performing this seemingly impossible task is discussed in Refs 17 and 18 and is treated briefly in the following section.

g. The RENT Raman Instrumentation

A schematic diagram of the LRS instrumentation used for the present arc-tunnel measurements is shown in Fig. 11; physical locations of some of the components may also be seen in Fig. 10. The light source was a Model C102 Avco Pulsed Nitrogen Laser, which produced 10-nanosecond half-width, 100-kilowatt pulses at a variable rate up to 100 pulses per second and delivered a maximum average power of 0.1 watt. The unpolarized ultraviolet laser output was at a wavelength of 3371 Å with an output bandwidth of 1 Å. The beam quality was poor since the raw beam had a rectangular cross section with initial dimensions of 1/8" x 1-3/8" and the beam divergence was quite large. When focusing the beam, two images formed across the smallest dimension, resulting from the laser cavity electrode configuration. Defocusing the image produced the best beam quality; however, the defocused beam width was not diffraction limited. Also, the laser output was not strictly monochromatic due to the spontaneous emission of nitrogen. The polarization, beam quality and spontaneous emission deficiencies of the N_2 laser source were offset by its high average power in the ultraviolet and its narrow pulse width. Also, Figs. 8 and 9 show that the choice of the N_2 ultraviolet laser largely avoided regions of strong flow background emission in arc-heated air flows. Further, in this wavelength region no significant absorption of incident or Raman radiation was expected by

the gas flow constituents, except possibly by NO_2 in the mixing regions at the edges of the tunnel hot air jet.

The remaining system design considerations were aimed at minimizing some undesirable features of the laser choice. For example, as shown in Fig. 11, a filter may be used in front of the laser to block unwanted radiation from the N_2 spontaneous emission in order to obtain a more nearly monochromatic source. The transmission of the filter was 61% at the laser frequency and 0.05% at 3577 Å, which is the location of the strongest emission band. This blockage becomes critical in Raman scattering experiments in oxygen since at 3577 Å the N_2 (0,1) band emission could interfere with the Raman O_2 (0,1) Q-branch radiation near 3558 Å.

The laser had to be located 26 feet from and downstream of the measurement point as shown in Fig. 10 in order not to interfere with the high priority RENT tests. Hence, a somewhat complex and non-optimum "transfer and focus" optical system had to be employed. The system consisted of a flat mirror, shown being adjusted in Fig. 10, which reflected the laser beam into a 6-foot focal length spherical mirror. The focused light from the spherical mirror gave an image size of about 2 mm x 1.3 cm at the tunnel centerline just downstream of the nozzle exit.

The intensity of the laser source was monitored by an RCA 1P28 Phototube after the beam had passed through the tunnel flow region in order to determine if any of the incident beam radiation had been absorbed by the test gas. A narrow band-pass filter, centered at 3371 Å and located in front of the 1P28 phototube, insured that affects of flow radiation would be reduced. The phototube output pulses were fed to a PAR Model 160 Box Car Integrator, which was triggered by synchronous pulses from the laser trigger generator. Integrator gate times of 30 nanoseconds were employed to provide a laser beam pulse height analysis while rejecting steady state background radiation by a factor of 3×10^5. The analog output of the gated integrator

was then plotted versus time during a tunnel run. Linearity of the system was checked by inserting various neutral density filters into the beam path and recording the integrator output voltage change. The elimination of flow radiation affects was confirmed through measurements made by the monitoring system before, during, and after a tunnel run.

Raman photons scattered vertically upwards were reflected 90° by a mirror which, based on RENT facility non-interference considerations, was positioned on an I-beam 58 inches above the test section. The photons were then collected by a 4-inch diameter f/23 collector lens (see Fig. 10) located 92 inches from the scattering volume, all of which resulted in a poor collection efficiency. However, the optical reduction of the scattering volume was such that the poor quality 2-mm beam width was reduced to 500 μm when imaged on to the spectrometer slit. This image size matched the slit width. Thus, a fraction of the Raman intensity lost due to the small solid angle of the collection optics was recovered by a decrease of the poor beam quality effects.

A low wavelength pass filter was placed in front of the spectrometer slit. The purpose of this filter was to block radiation of wavelengths higher than the Raman region in order to reduce scattered light problems arising inside the spectrometer. A Corning Glass Filter No. C57-51 was used in this experiment. The No. 51 filter passes 78% of the light in the Raman Stokes region and has good blockage properties between 4300 Å and 6600 Å. Beyond 6500 Å the RCA 8850 PMT, which was used in conjunction with the spectrometer, has a negligible spectral response, and so adequate blockage of all radiation above 4300 Å was accomplished using this filter-PMT combination. A second filter labeled DDDP in Fig. 11 was employed in front of the photomultiplier tube to block scattered light at, and below, the laser wavelength. This liquid filter has the

property of essentially complete isotropic absorption at 3371 Å but nearly complete transparency at wavelengths of 3500 Å and longer.[17]

The spectral analyzer used in the present experiment was a 1/4-Meter Jarrell-Ash Ebert Scanning Spectrometer. It was operated in the first order with 500 μm slits and a 1180 grooves/mm grating blazed at 3000 Å, giving a spectral bandpass of approximately 19 Å. The f/3.5 aperture ratio of the instrument provided good light gathering capabilities. Also, the small size and light weight of the spectrometer made it quite suitable as a practical measuring device for the present wind tunnel diagnostics study.

The basic Jarrell-Ash instrument was altered to enable remote selection of several fixed wavelengths within the Raman spectral region. This was accomplished by placing mechanical stops on a pulley attached to the wavelength drive screw of the spectrometer. Remote rotation of the wavelength drive was then accomplished with a Selsyn transmitter-receiver combination. The stops contacted either side of a retractable plunger, which provided a fixed wavelength choice for both clockwise and counterclockwise pulley rotation. Remote retraction of the plunger by a linear solenoid enabled other pairs of stops to be used, so that more than two known wavelengths could be remotely selected by using the "Selsyn" in conjunction with the solenoid.

Several drawbacks of the 1/4-meter instrument should be noted. The wavelength dial could be visually set to an accuracy of only 2 Å in the first order. Linear interpolation had to be used for wavelength settings between the 2 Å dial rulings. Hence, a careful calibration was required to enable accurate wavelength selection at the mechanical stops. Also, the internal scattered light properties of the instrument were poor. However, the use of a broad slit width, which implies a broad apparatus function, reduced the effects of wavelength setting

inaccuracy and, as mentioned above, the application of filters reduced the significance of the scattered light problems.

The spectrometer apparatus function $A(\Delta\lambda)$ of the present instrument configuration is shown in Fig. 12. It was obtained by taking an average of the spectral profiles of four mercury lines from a low pressure Pen-Ray lamp source. The Hg lines were assumed to be delta functions, so the apparatus function could be obtained directly from the PMT output plot. A Keithly picoammeter was used as the output measuring device. Note that the curve fit of $A(\Delta\lambda)$, which is necessary for the calculation of theoretical Raman profiles, is in the form

$$Y = 10^{c_0 X + c_1 X^2 + \cdots c_k X^k} \qquad (23)$$

where k=16 gave the best fit of the profile data. A regular polynomial fit cannot be used directly for spectrometer apparatus functions due to the shape of the wings of the profile. The ability of Eq (23) to fit $A(\Delta\lambda)$ is obvious from Fig. 13, where the log $[A(\Delta\lambda)]$ versus $\Delta\lambda$ is shown to plot in a polynomial form. The erratic behavior of the log-curve fit near the wing tips resulted from the curve fitting process itself and was avoided by restricting $\Delta\lambda$ to values within the well behaved regions of the fit.

An RCA 8850 Quantacon Photomultiplier Tube was employed to convert the spectrally analyzed photon flux into a photoelectric pulse having a half-width approximately equal to the laser pulse half-width of 10 nanoseconds. This signal pulse was then fed into, and analyzed by, an electronic network. Due to the narrow pulse width requirements, the dynode chain and plate circuitry was designed to operate the tube in the fast pulse response mode. Rise times of 2 nanoseconds were expected. The RCA 8850 PMT was selected because of its high gain and expected excellent quantum efficiency of 30% in the Raman Stokes wavelength region. The tube was operated at 1950 volts, which

resulted in a high quality pulse amplification of 10^7 through the dynode chain. This amplification was necessary to produce signal pulses which could be recognized by the pulse discrimination electronics.

The pulse analysis system shown in the block diagram of Fig. 11 consisted of a combination of off-the-shelf ORTEC Nuclear Instrumentation Modules (NIM) and was designated as the SPEC (Single Photoelectron Counting) System in Fig. 11. The purpose of the system was to recognize and count laser Raman scattered photoelectrons from among those produced by PMT thermionic emission or continuous flow background radiation. The SPEC electronics system was quite similar to ordinary photon counting instrumentation except that it was designed for use with fast pulsed lasers. Here, fast is in the sense that existing photon counting equipment could not distinguish multiple photoelectric events during the short laser pulse lifetime. Hence, the SPEC system works on what might be called the 1-0 principle. That is, each incident laser pulse must produce either only one photoelectron event or none at all at the PMT cathode. The 1-0 principle is applicable only in the low Raman intensity regime, which was expected in the arc-tunnel experiments. The single photoelectron counting electronics were chosen to provide gating capabilities (i.e., pulse resolution) of the order of 10 nanoseconds while handling an input count rate of up to 20 MHz. Hence, the system was capable of reducing the dark current and flow background emission by a factor of 10^6.

The heart of the SPEC system is the ORTEC Model No. 447 Time-to-Pulse-Height Converter. The laser trigger synchronous timing pulse started the time-to-pulse-height converter, and the scattered Raman photoelectron pulse stopped the instrument. This converter transformed the time elapsed between the "start" and "stop" inputs into a proportional analog output

voltage between 0 and 10 volts. If no "stop" pulse arrived during the gate time of 50 nanoseconds, the instrument was reset (i.e., readied for another start pulse) and no output pulse was produced. Hence, the capability of detecting Raman photoelectrons with 50-nanosecond resolution was accomplished with this instrument alone, provided the proper input pulses were received and the timing could be adjusted to insure that the Raman pulse arrived within the gate time. This timing, as well as pulse conditioning, was performed by several other of the SPEC instruments. An Ortec Model No. 454 Timing Filter Amplifier amplified the pulse signal by a factor of 200 in preparation for subsequent processing. A differential time constant of 10 nanoseconds was employed to insure up to 20-MHz pulse handling capability. The output of the timing filter amplifier was fed into an Ortec Model No. 436, 100-MHz Discriminator. This instrument was adjusted to reject amplifier noise and photoelectric pulses originating within the dynode chain rather than at the cathode. All the pulses above the discrimination level were converted to standard fast logic pulses. Since remote operation of the equipment was required during the arc tunnel testing, the Ortec No. 454 and No. 436 instruments were located near the photomultiplier tube in order to avoid any difficulties which could be encountered due to long cable transmissions, while the remainder of the instruments were located in a less hazardous and more remote area. Thus, a 100-foot cable was required to transmit output pulses from the No. 436 instrument to the "stop" input of the No. 447 instrument.

The laser also was located in the test area, as described above, so another 100-foot cable was required to transfer the synchronous timing pulse necessary for selection of only laser scattered photons. Since the laser timing pulse was not suitable for feeding directly into the "start" input of the No. 447 instrument, an Ortec Model No. 416A Gate and Delay Generator was employed for pulse conditioning. The No. 416A instrument produced a standard fast logic pulse for each input

pulse from the laser trigger generator. The time between the arrival of the laser trigger pulse and the Raman pulse was of the order of 1 microsecond. Hence, the No. 416A was also employed to delay the starting of the No. 447 by producing the "start" pulse at the proper time after the synchronous timing pulse had arrived.

The combination of instrumentation described above enabled discrimination of Raman from other photoelectrons to within 50 nanoseconds. In order to improve further the pulse resolution of the SPEC system, an Ortec Model No. 406A Single Channel Analyzer (SCA) was connected to the output of the No. 447. The upper and lower discriminator levels on the SCA were set such that only start-stop combinations which resulted in the proper amplitude range would produce standard pulses at the output of the SCA. Hence, 10-nanosecond gate times were attainable using the SCA in combination with the time-to-pulse-height converter. Finally, the standard pulses produced by the SCA were counted by an Ortec Model No. 449 Rate Meter. The analog output of the rate meter was then plotted versus time on an X-Y recorder.

In a pre-RENT test trial, the ability of the SPEC electronics to drastically reduce the continuous background radiation was checked by exposing the PMT to various arbitrary light signals of about the same intensity as expected from flow radiation during the arc-tunnel tests. The trigger generator was pulsed at 100-Hz, and a 100-nanosecond gate time was employed, which implied a noise reduction factor of 10^5. The anode current was measured with a picoammeter. The anode count rate and the rate meter reduced count rate were also recorded. However, due to the count rate limits of the rate meter, only a limited amount of anode count rate data was obtained. The experimental results are shown in Fig. 14. Note that, indeed, the expected reduction of background signal was achieved and the electronic gating method was validated. The

linearity of the data also demonstrates that the system was capable of properly handling the higher count rates which were expected to be encountered in the arc-tunnel test environment.

The RENT Raman instrumentation system as described above yields the following values for system parameters which were used to calculate the expected count rate N_{pe} from N_2 Raman scattering in room air:

TABLE I

Parameter	Value Assumed	Explanation
N_i	2.4×10^{16} photons/sec	This value corresponds to the horizontally polarized portion of the total 75-mw measured average power after double reflection and focusing. The laser repetition rate was 100 pps.
σ	2×10^{-30} cm^2/particle-sr	Value from Ref 19 and corrected for wavelength variation.
n	1.86×10^{19} particles/cm^3	Nitrogen number density in room air; expected to increase slightly during test.
Ω	1.4×10^{-3} steradians	Solid angle for f/23 optics.
ℓ	2.5 cm	Measured field of view of receiver optics.
ϵ	0.05	Total measured transmission factor of collection and analysis optics at 3650 Å: Collector mirror 0.70 Glass collector lens 0.78 Spectrometer 0.10 DDDP filter 0.87
Q_e	0.2	Actual quantum efficiency of RCA 8850 PMT photocathode.
$T_{\lambda_{ex}}, T_{\lambda_{Ram}}$	1	This transmission factor will vary somewhat for run conditions.

Substituting the above values into Eq (17) showed that N_{pe}=30 counts/sec was to be expected in the RENT tests. Although the design value seems low, it is noted that no more than 50 counts/sec could be reliably obtained using the present 100-pps laser because the 1-0 principle would be violated as the count rate increased above 50.

SECTION V

DISCUSSION OF RESULTS

1. ROOM TEMPERATURE DATA

Raman scattering data at ambient conditions were obtained in the laboratory environment at ARL and in the arc facility itself. The optical f/-number, spectral slit width, and electronic gate values used were typical of the arc-tunnel flow experiments which followed. The purpose of these room temperature measurements was to validate the single photoelectron counting system for Raman scattering diagnostics and to check the Raman theory used in the temperature and number density determinations.

The SPEC system and the limits of the 1-0 principle were checked by making N_2 Raman Q-branch peak intensity measurements in room air at various pressures from 1 to 7 atmospheres. The results of these measurements, made under laboratory conditions, are shown in Fig. 15. Note that the measured Raman intensity varied linearly with pressure at constant temperature. This linear variation, which is the basis for number density determination, indicated that the SPEC system operated properly. Also, the linear variation of count rate with pressure, shown in Fig. 15, persisted even up to half the laser repetition rate of 100 pulses/sec. Hence, the 1-0 principle is valid up to the arbitrary limit set at 50% of the laser pulse rate. Beyond this limit, nonlinear effects of multiple photoelectric events per laser pulse would have become apparent.

Also, Raman spectral intensity measurements at ambient conditions in the AFFDL RENT Facility were compared with calculated Raman profiles. This comparison was made to determine the room temperature count rate and to ascertain which features of the Raman theory should be included for the particular experimental setup of the arc-tunnel test. The N_2 Raman intensity data were obtained by selecting wavelengths within the region of interest and allowing sufficient time for a steady

state signal to be obtained. Observed fluctuation of the signal was attributed to photon statistics, and the values plotted in Fig. 16 are time averages of the count rate at a particular wavelength value. Along with the scan data, intensity values were obtained at particular wavelength values dictated by the mechanical stops on the spectrometer wavelength adjustment mechanism.

The comparison of relative intensity profile experimental data with that obtained through theoretical computations is also shown in Fig. 16. Note that, for the broad spectrometer apparatus function used in the present experiments, the O- and S-branch satellite transitions must be included along with the Q-branch transitions to obtain close correspondence between theory and experiment. This is especially true near the wings of the profile.

The peak intensity value of $N_0 = 14$, used to normalize the above spectral data, was one-half that expected from photoelectron count calculations found in Section IV.2.g. This discrepancy could have been caused by the cumulative effects of experimental errors in measuring the various parameters. Also, it was discovered after completion of the tests that the receiver mirror was slightly bent in its mount so that the solid angle Ω was less than estimated. In general, the measured count rate was lower than desirable. This resulted in several experimental difficulties noted below.

Photon statistics imply that

$$N_T = N_m \pm \sqrt{\frac{N_m}{2}} \qquad (24)$$

where N_m and N_T are the measured and true count rates, respectively. Hence, the signal-to-noise ratio in photon counting application is written as

$$S/N = \frac{N_m}{\sqrt{N_m}} = \sqrt{N_m} \tag{25}$$

and the error introduced by the statistical nature of the photoelectric effect is given by

$$\% \text{ Error} = 100 \frac{\sqrt{N_m}}{N_m} = \frac{100}{\sqrt{N_m}} \tag{26}$$

Equations (25) and (26) show that larger count rates imply greater accuracy. For $N_0 = 14$ counts/sec an integration time (i.e., counting period) of 2 seconds is necessary to obtain 20% data accuracy while 7 seconds is required for 10% accuracy in the Raman intensity measurement. Therefore, low count rates must be compensated through longer measurement times. This implies that only time averaged measurements, taken over the total time required to gather sufficient data, for reasonable accuracy, can be obtained at low count rates. In the present case, the measured count rate was too low to allow use of the long wavelength blocking filter.

2. ARC-TUNNEL SPECTROSCOPIC MEASUREMENTS

Some of the difficulties with making spectroscopic measurements in arc-heated flows are discussed in Section II. Of those mentioned, background flow emission and incident laser beam absorption proved to be the major problems. Electrostatic, magnetic and acoustic noise was eliminated by various shielding methods. Double shielded cables and a mu-metal PMT shield proved most effective in overcoming the electrostatic and magnetic noise. Enclosing the spectrometer in a plywood box lined with acoustical insulation eliminated the acoustic

vibration problem. Also, short tunnel-run-time problems were circumvented by using the rapid wavelength selection method, involving the rotary-drive mechanical stop system. Hence, adequate time was available to obtain the basic spectroscopic data.

The magnitude of the flow radiation problem was of primary concern during the arc-tunnel tests. However, since identification of the radiation source also was important, several spectral scans in the region from 3500-3800 Å were made to identify this source. Results of these scans are shown in Fig. 17. It should be noted that the count rates in Fig. 17 are not actual, but rather, effective values. That is, the true background count has been reduced by a factor of 10^6 by the pulsed laser-gated photon counting system. It is this effective background count rate which will tend to mask the predicted Raman signal of approximately 15 counts per second. During run No. 35-004 and No. 35-006, indicated in Fig. 17, the Corning No. C57-51 high lambda blocking filter was employed in conjunction with the permanent DDDP laser line blocking filter. The spectrometer was continuously scanned through the Raman region of the spectrum. Note that the flow radiation was strongest at the lower wavelengths. This suggests that the radiation is due to the broadened wings of the nearby copper resonant doublet at 3248 Å and 3274 Å. The double filtered scans also show that background radiation interference for O_2 vibrational Raman scattering near 3558 Å is approximately three times more serious than for N_2 scattering near 3658 Å. The No. C57-51 filter was later removed due to the low Raman count rate restrictions mentioned earlier. Further spectral scans were then obtained without the high lambda blocking filter during run No. 38-017. The unfiltered scan during this run exhibited no wavelength dependence. This was possibly due to scattered light inside the spectrometer from previously blocked flow radiation at wavelengths greater than 3800 Å which was not detected by the PMT. Hence, absence of

the No. C57-51 filter worsened the background radiation problem in the N_2 Raman spectral region. The radiation at these higher wavelengths could be due to any or all of the sources mentioned in Section III.2.

Also plotted in Fig. 17 are effective background radiation count rates at various wavelength locations obtained during several other arc-tunnel runs. These data points show that the amount of background radiation in the N_2 Raman region does not correlate with gas pressure, as can be seen from the wide variation in effective count rate for constant stagnation pressure. Hence, the dominant radiation is probably not due to NO chemiluminescence or NO band spectra. Either gas radiation from copper electrode vapor in the stagnation section (i.e., flash light effect) or copper line radiation itself is apparently the dominant source. Since the double filtered spectral scans do exhibit the behavior noted above, copper line radiation is probably the dominant radiator in this high pressure-high enthalpy arc tunnel flow. This observation agrees with rapid scan data taken in the RENT Facility by Lawrence.[20] In addition, physical examination of the test models after a particular test showed more copper particle pitting of the nose tips for the high flow radiation runs. In fact, runs No. 38-005 and No. 38-017 were unsuitable for testing models due to this pitting problem. Hence, the effective flow copper vapor radiation was less than 8 counts per second for usable tunnel runs. This gives a predicted signal-to-background ratio of at least 2 to 1.

Some of the incident laser beam energy and the scattered Raman radiation was absorbed by the flow. The magnitude of this effect can be seen from the absorption measurement results shown in Fig. 18. Note that at worst the measured beam attenuation was 13%. This was for the unusable run due to copper pitting of test models. For the usable runs the absorption was less than 7%. Also, Fig. 18 shows that the attenuation was directly proportional to the measured copper

vapor radiation. Hence, the absorption is most likely due to the presence of the copper electrode material in the test gas. The stagnation pressures were constant for the run data plotted in Fig. 18, so molecular NO_2 or H_2O absorption was negligible since the amount absorbed does not notably depend on the concentration of these species. Again, the physical evidence of copper pitting of the models during run No. 38-005 leads one to suspect that copper vapor was indeed the absorber.

3. RAMAN SCATTERING MEASUREMENTS IN ARC-HEATED FLOW

After sufficient static and flow background data were obtained, a Raman scattering measurement was attempted under arc-tunnel flow conditions. Pre-run calibrations were made of the relative incident laser beam intensity and the Raman signal from nitrogen in the room air. These calibrations, which were obtained within 30 seconds of the tunnel run, were made to assure that the electronic instrument delays were properly adjusted and to obtain a calibration point for use in the determination of the flow N_2 number density and the laser beam absorption.

A tracing of the raw data obtained prior to, and during, a typical arc-tunnel run (run No. 38-006) is shown in Fig. 19. The laser power output and rate meter signal were simultaneously recorded versus time. Note that some data on laser beam attenuation, flow background radiation and nitrogen Raman scattering were obtained before the test models were injected into the flow and some obtained after the models were retracted.

The pre-run laser power, which is labeled in Fig. 19, was obtained by recording the gated integrator output with the laser alternately on and off. To obtain the Raman calibration, the output of the rate meter was recorded with the laser on and the spectrometer set at $\lambda = 3662.5$ Å. This setting was near the peak intensity wavelength for room temperature N_2 Raman scattering of 3658 Å. The recorded count rate is labeled

PRERUN (1) in Fig. 19. Also, the count rate was recorded at wavelength λ_3 = 3719.5 Å, which was outside the Raman region and therefore represented the effective zero point for the Raman calibration. Hence,

$$\text{Raman } N_2 \text{ Calibration Count Rate} = \text{PRERUN } (1) - (3) = 11 \frac{\text{counts}}{\text{sec}} \qquad (27)$$

Note that the PRERUN (3) signal is approximately 6 counts/sec greater than the zero Raman which was obtained with the laser off and the room lights turned off. Thus, some noise can be attributed to the laser pulse generator and/or the high intensity flood lights which were used in photographing the test models. To determine the amount of noise from each background source, a remotely operated shutter, which blocked all light from entering the spectrometer slit, was actuated while the laser was on. The count rate dropped to the value labeled SHUTTER CLSD in Fig. 19. Hence,

$$\text{Flood Light Noise} = \text{PRERUN } (3) - \text{SHUTTER CLOSED} = 2.5 \frac{\text{counts}}{\text{sec}} \qquad (28)$$

Thus, 2.5 of the 6 noise counts/sec were attributed to the flood lights. The remaining noise counts were due to the electronic noise generated when the laser high voltage pulse generator discharged energy into the laser cavity through the exposed coaxial cables. Since this noise source is nearly coincident to and is synchronized with the Raman signal, it is difficult to avoid. (The newer models of the Avco nitrogen pulsed laser have enclosed cables between the pulse generator and the cavity which should significantly reduce this noise level.)

After completion of the prerun calibration, the spectrometer was reset to $\lambda = \lambda_1$. The arc-tunnel was started and approximately 30 seconds later was "on condition." The plotter, after being reset to zero time, was then started, and after 8 seconds the wavelength position was changed to λ_2 = 3643.5 Å

(i.e., ① - ② as labeled on the plot in Fig. 19). Again, after 8 seconds had elapsed, the spectrometer wavelength was set to λ_3 (i.e., changed from ② - ③). At approximately the same time as the change to position ③, the first of 5 test models was injected into the flow. The models physically blocked the laser beam for brief periods, as can be seen by the sudden changes in the laser power monitor output. After the last test model was out of the flow and the laser power indicator was back to a steady value, 8 seconds were again allotted for measurement of the count rate at wavelength position ③ shown in the plot. Using Eq (27),

$$\text{RUN RAMAN} = \text{RUN } ① - \text{RUN } ③ = 3.5 \frac{\text{counts}}{\text{sec}} \tag{29}$$

The laser was then turned off while the tunnel continued to run for approximately 8 seconds longer. The count rate dropped due to the removal of the laser induced noise mentioned above. The tunnel run was then terminated, and the count rate dropped again to the 2.5 counts/sec level associated with the model photography flood lights. The difference between the laser-off/tunnel-on count rate and the flood light background count rate was due to the flow background emission. Hence, the flow radiation contributed approximately 7 counts/sec to the ratemeter signal. Note that the laser beam output was approximately 10% less during the run than the value recorded in the prerun power measurement. Also, the beam attenuation was constant during the recording of output at wavelengths λ_1 and λ_2, so a correction for laser output drift was not necessary.

To infer the number density and vibrational temperature of molecular nitrogen from the above raw arc-tunnel data, further theoretical computations of the Raman intensities at λ_1 and λ_2 were required, using the actual apparatus function shown in Fig. 12. The results of these calculations for various temperatures are shown in Fig. 20. It is noted that thermodynamic equilibrium (i.e., $T_V = T_R = T$) was assumed to exist among

the vibrational, rotational and translational energy modes for these calculations and only Q-branch Raman transitions were used to generate the computer plots shown. Calculations which included O- and S-branch transitions also were made, and the results of several ratios of N_2 Raman intensities at λ_1 and λ_2 are shown in Fig. 21 for the Q-branch alone and for the Q-, O- and S-branch cases. It was found that the satellite transitions must be included in this calculation in order to obtain accurate temperature determination below 2500°K and in order to make proper number density corrections for temperatures above 700°K. However, the addition of the O- and S-branch transitions may not be required for other experimental conditions (i.e., narrower apparatus functions and different λ_1-λ_2 combinations). Each specific case must be checked to determine if the $\Delta J = \pm 2$ transitions may be neglected.

The plots in Fig. 20 show that the Raman intensity I_{λ_2}, labeled (2) at 3643.5 Å, is quite sensitive to vibrational temperature above 1000°K. Further, the intensity I_{λ_1} is much less sensitive to temperature change. Hence, this $I_{\lambda_2}/I_{\lambda_1}$ ratio, which is shown in Fig. 21, can be used to determine the vibrational temperature of the gas independently of number density. Also, the $I_{\lambda_1}(T)/I_{\lambda_1}(300)$ ratio for constant number density can be used to correct for temperature effects on the arc tunnel number density determination.

From the data in Fig. 19:

$$I_{\lambda_1} = 28 \text{ counts/8 seconds } \pm 2.6 \text{ counts}$$

$$I_{\lambda_2} = 4.1 \text{ counts/8 seconds } \pm 1 \text{ count}$$

$$\frac{I_{\lambda_2}}{I_{\lambda_1}} = 0.15 \pm 0.05$$

Hence, the vibrational temperature determined from Fig. 21 was less than 600°K for the arc-tunnel tests. It could not be determined more closely than this due to the data scatter

caused by poor photon statistics at low count rates and the insensitivity of this particular measurement at low temperatures.

Substituting the number density data from Fig. 19 into Eq (16), where

$$I(3662.5)_T = 28 \pm 2.6 \text{ counts/8 seconds}$$
$$I(3662.5)_{300} = 88 \pm 4.7 \text{ counts/8 seconds}$$
$$n_{STAND} = 1.86 \times 10^{19} cm^{-3}$$

gives

$$n_{N_2} = 5.9 \times 10^{18} cm^{-3} \pm 15\%$$

Fig. 21 shows that a temperature correction for the above value is unnecessary at the low measured temperature. However, a correction must be made for the laser beam absorption. The magnitude of the correction is approximately $(1-\alpha_1/2)^2$, where $\alpha_1 = 0.10$ from data in Fig. 18. Thus,

$$n_{N_2} = 6.5 \times 10^{18} \text{ cm}^{-3} \pm 15\%$$

Hence, the arc-tunnel Raman results are:

TABLE II

Quantity	Calculation	Raman Measurement
$T_{v_{N_2}}$	3570°K	<600°K
n_{N_2}	2.7×10^{19}	$0.65 \times 10^{19} \pm 15\%$

The comparison of theory with experiment shown in Table II above indicates that the measured temperature was much lower than expected from equilibrium calculations performed by the Flight Dynamics Laboratory. Also, the number density was one fourth the theoretical value.

A plausible explanation of the poor comparison of theory with experiment may be that the actual measured values were spatial averages of a large portion of the radial profile rather than point measurements of centerline values, as assumed in the theoretical calculations. This point is illustrated in Fig. 22, which shows the determination of the spatial resolution of the

optical system. The data were obtained by moving a Pen-Ray lamp across the 1.1-inch diameter RENT nozzle exit and recording the PMT output with the spectrometer set at the 3650.2 Å Hg wavelength position. Note that radiation from radial distances as much as an inch from the centerline was gathered by the optics. Further, the scattering volume observed was located 0.45" downstream of the nozzle exit, as shown by the slit image and nozzle exit scale drawing in Fig. 22. Hence, Raman scattered photons from the cooler regions outside the test rhombus also were being collected and analyzed by the measurement system. Therefore, the temperature inferred from these measurements could be considerably less than a centerline value.

The above explanation does not, however, apply to the number density discrepencies since this parameter should be nearly constant across the jet for the particular run conditions of the present tests. Perhaps mechanical vibration , with could cause misalignment of the receiver optics and the incident beam path, was responsible for the lower measured signal. Of course, vibration would not affect the temperature measurements since only relative intensities are required. Finally, the above measurements were made with the facility operating in the peaked enthalpy profile mode discussed above. This condition further compounded the spatial resolution problem since only a small region in the center of the flow may have possessed the theoretically expected conditions. Measurements should also have been made for a flat enthalpy profile case. Unfortunately, no flat profile runs were scheduled during the time of the Raman measurements.

4. CONSIDERATION OF EXPERIMENTAL IMPROVEMENTS

Improvements of the present experimental setup, which could not be performed due to time limitations, center around approaches toward increasing the Raman count rate. Once the signal is increased, other favorable modifications also can be made.

In Table I, the number of incident photons/sec actually corresponds to only 14 milliwatts of average laser power at 100 pulses/sec in the proper plane of polarization. This low figure arises from the fact that the measured total laser power was only 75 milliwatts instead of the rated value of 100. Also, double reflection from the uncoated focusing system optics resulted in only a 40% overall reflectivity. An off-the-shelf Avco C-5000 500-Milliwatt Pulsed Nitrogen Laser is available at the present time. This new laser coupled with anti-reflective coatings of the focusing mirror system could deliver about 200 milliwatts of power at 500 pulses/sec in the proper plane of polarization. This represents a factor of 14 gain in Raman signal while increasing the background count rate by a factor of only 5. Another advantage of this new laser is the higher maximum repetition rate of 500 pulses/sec. This means that about 250 counts/sec could be measured without violating the 1-0 principle, instead of only 50 using the present C-102 model laser. Hence, similar statistical accuracy would be obtained in 1/5 the time using the 500 pps laser. Also, the new Avco C-5000 model laser has improved shielding properties and the laser discharge noise source would be minimized. Finally, it appears likely that polarization of the laser beam, together with proper design of the optical system to account for polarization effects, could lead to a Raman signal gain.

To further increase the Raman count rate by increasing the solid angle and optical efficiency would increase also the background radiation by an equal amount. However, once the signal is increased, measures could be taken to reduce selectively the background contribution to a greater degree than the Raman signal is attenuated. An f/12 optical system, which is within the physical constraints of the RENT Facility test chamber, utilizing lenses and mirrors, could be employed. Anti-reflection coatings on this system could increase the total collection efficiency at least fivefold. Also, the present spectrometer efficiency was only about 10%, based on a

conservative estimate. Hence, correcting this problem could increase the overall optical efficiency gain factor to about 10. The estimated overall gain in Raman signal from all the above improvements is 140 while the background signal increased only by a factor of 50. Following these changes aimed at increasing the signal strength, further modifications could be made to improve other performance aspects of the experiment.

The resolution of the optical system could be decreased by an order of magnitude to 0.1" (i.e., ℓ = 2.5mm); this would decrease the Raman signal and the flow radiation by similar amounts. Furthermore, since the Raman scattered radiation is nearly plane polarized, a Glan-Thompson prism could be used to halve the background radiation while reducing the Raman signal by only approximately 10%. Also, a high lambda blocking filter could now be used to reduce further the background radiation effects by perhaps another factor of 3 while attenuating the Raman signal again by about 10%.

The above improvement, if realized, would result in the following approximate count rates based on results obtained in this study:

Room temperature N_2 Raman = 150 counts/sec
Arc-tunnel Raman = 50 counts/sec
Arc-tunnel Background <5 counts/sec

Perhaps the removal of vibration effects (i.e., by more rigid and perhaps common mounts) would increase the Raman to background ratio even further and should be tried.

With the above count rates, data gathering would be greatly accelerated over the present rate. In the approximately 24 seconds of available run time, twelve spectral intensities could be obtained to within, at least, a 10% accuracy. This increased data gathering capability then would allow a stepper motor to be used on the spectrometer wavelength drive to provide a capability of rapid scan and stop at specific wavelengths

within the Raman rotation-vibration spectrum. At least 10 data points of intensity versus wavelength could be gathered in the same testing time, which would enable quite accurate determination of tunnel flow properties.

SECTION VI

CONCLUSIONS

The experiments described in this report demonstrate that it is feasible to make Raman scattering measurements in high pressure, high enthalpy, arc-tunnel flows. The results also suggest that measurements in low pressure facilities are possible. Hence, the experimental measurement of chemical and thermodynamic properties of the major molecular constituents in arc-heated flows, some of which were previously unattainable by direct means, should not be possible. This flow calibration method could also be used to evaluate the degree to which arc-facilities simulate free-flight conditions.

Theoretical calculations and Raman measurements at room conditions showed that, for broad apparatus functions and a judicious choice of wavelengths, a two channel data acquisition system could be employed to obtain independent measurements of molecular vibrational temperature and number density. Further, calculations revealed that under certain experimental conditions, O- and S-branch transitions must be included along with Q-branch transitions for accurate temperature and number density determination. These conditions occur (1) during the use of broad apparatus functions, and (2) while measurements are being made at wavelengths near the wings of the rotation-vibration spectrum.

Experimental measurements revealed that deleterious effects of acoustic and electromagnetic noise were present and could be overcome by isolating the measurement system from the arc-tunnel noise sources. Laser beam attenuation, which was shown in this experiment to be due to copper particles in the flow and copper vapor absorption, was a minor problem but was not negligible for some tunnel runs. The major and continuous experimental problem was found to be flow background radiation which tended to mask the Raman signal. For the particular

facility employed in this study, copper line radiation was identified as the dominant radiation source. The adverse effects of the above background noise were, however, adequately reduced by the Single-Photoelectron-Counting (SPEC) technique used in the data acquisition system.

Comparison of measurements of the vibrational temperature of nitrogen at the nozzle exit with equilibrium flow theory showed that the radially averaged temperature data obtained in this experiment could not be compared with a theory that predicts centerline values. Also, the discrepancies between theoretical and experimental number density noted in this study pointed out a need to study mechanical vibration effects on the instrumentation. Therefore, further measurements with an improved point measurement system must be obtained before qualitative comparison of theory and experiment can be made.

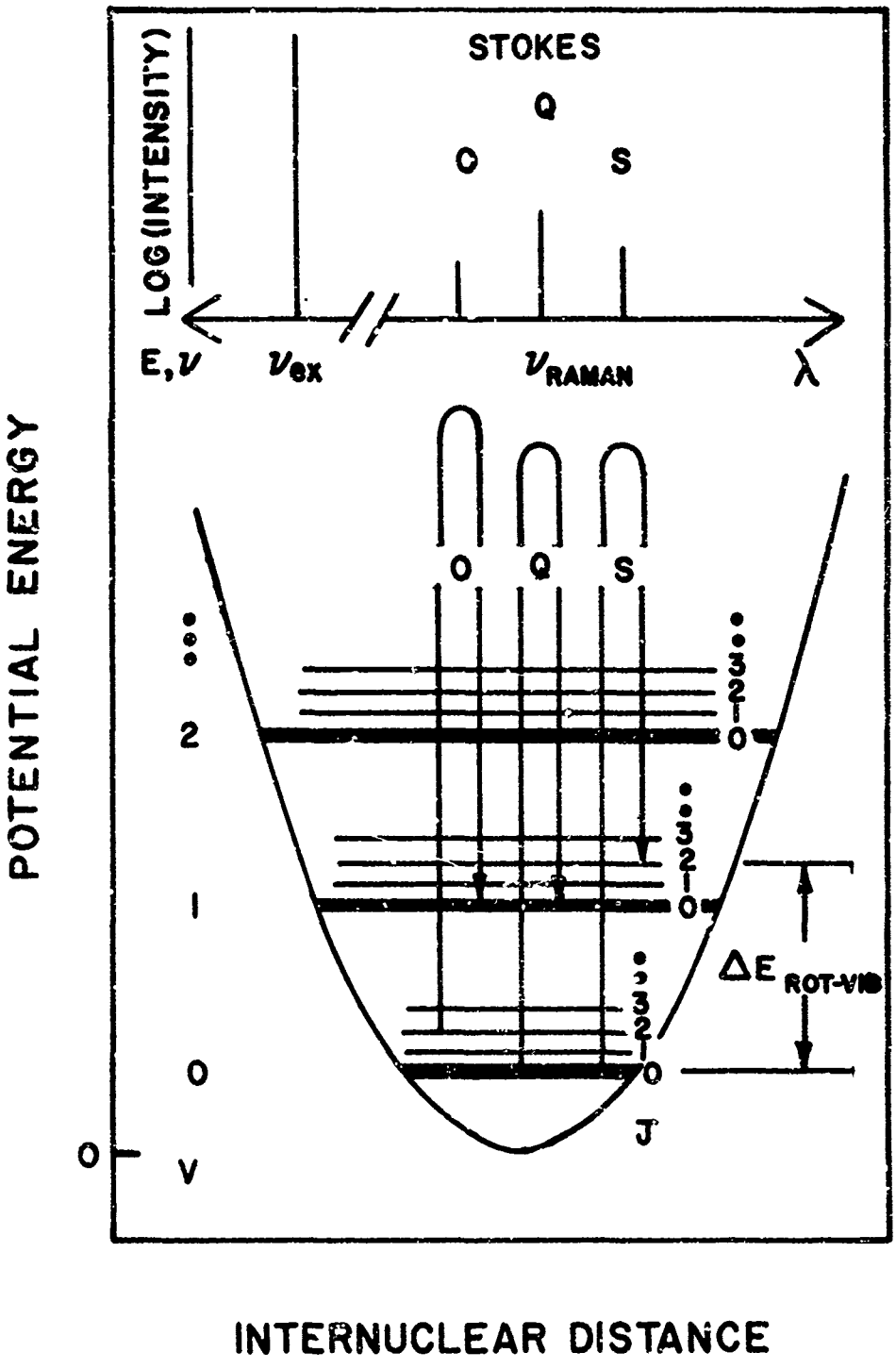

Figure 1. Energy Level Diagram Including Several Possible Raman Transitions and Corresponding Spectra.

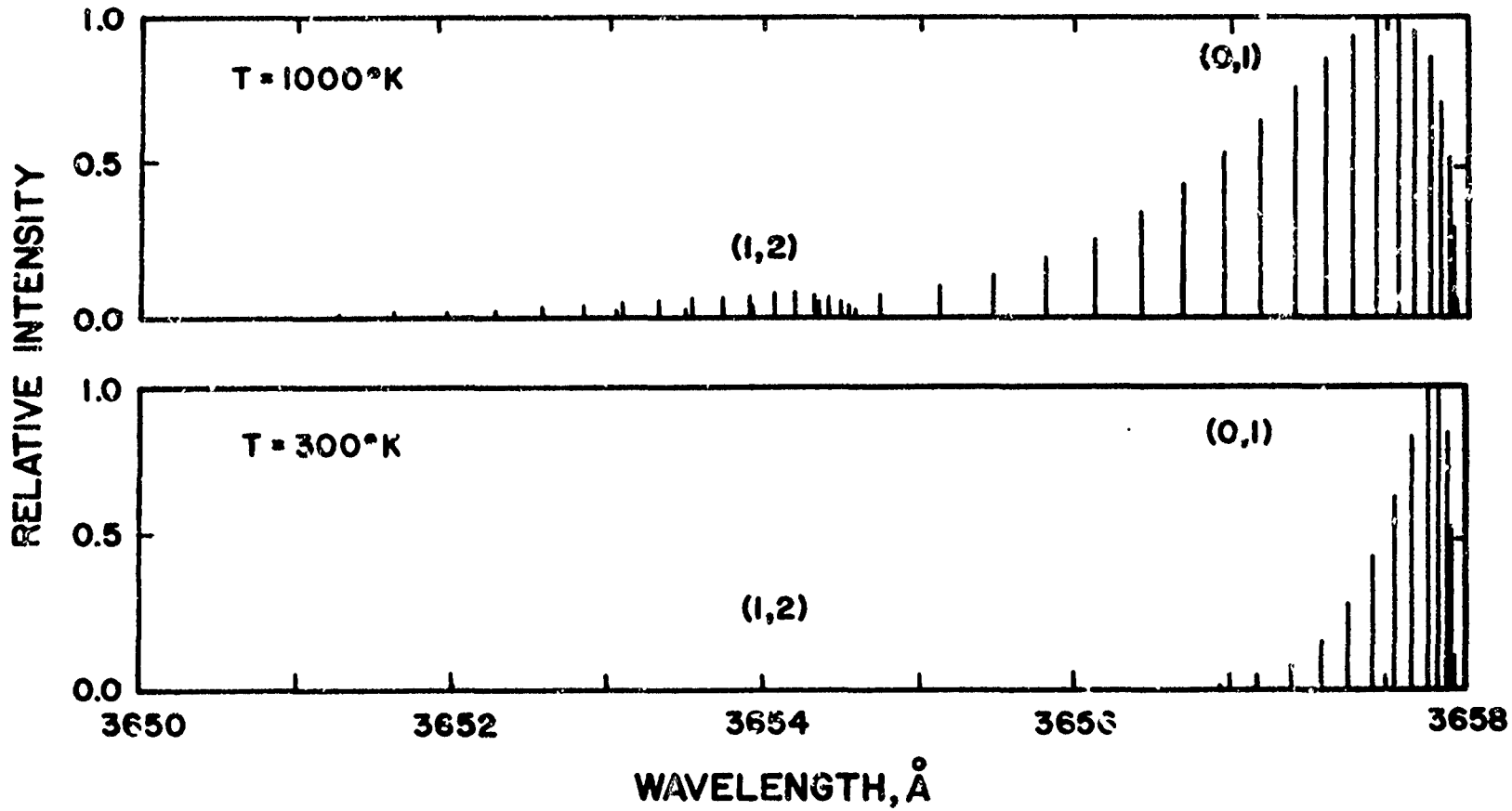

Figure 2. Calculated Rotation-Vibration Even J, Q-Branch Line Intensities for Molecular Nitrogen at 300°K and 1000°K.

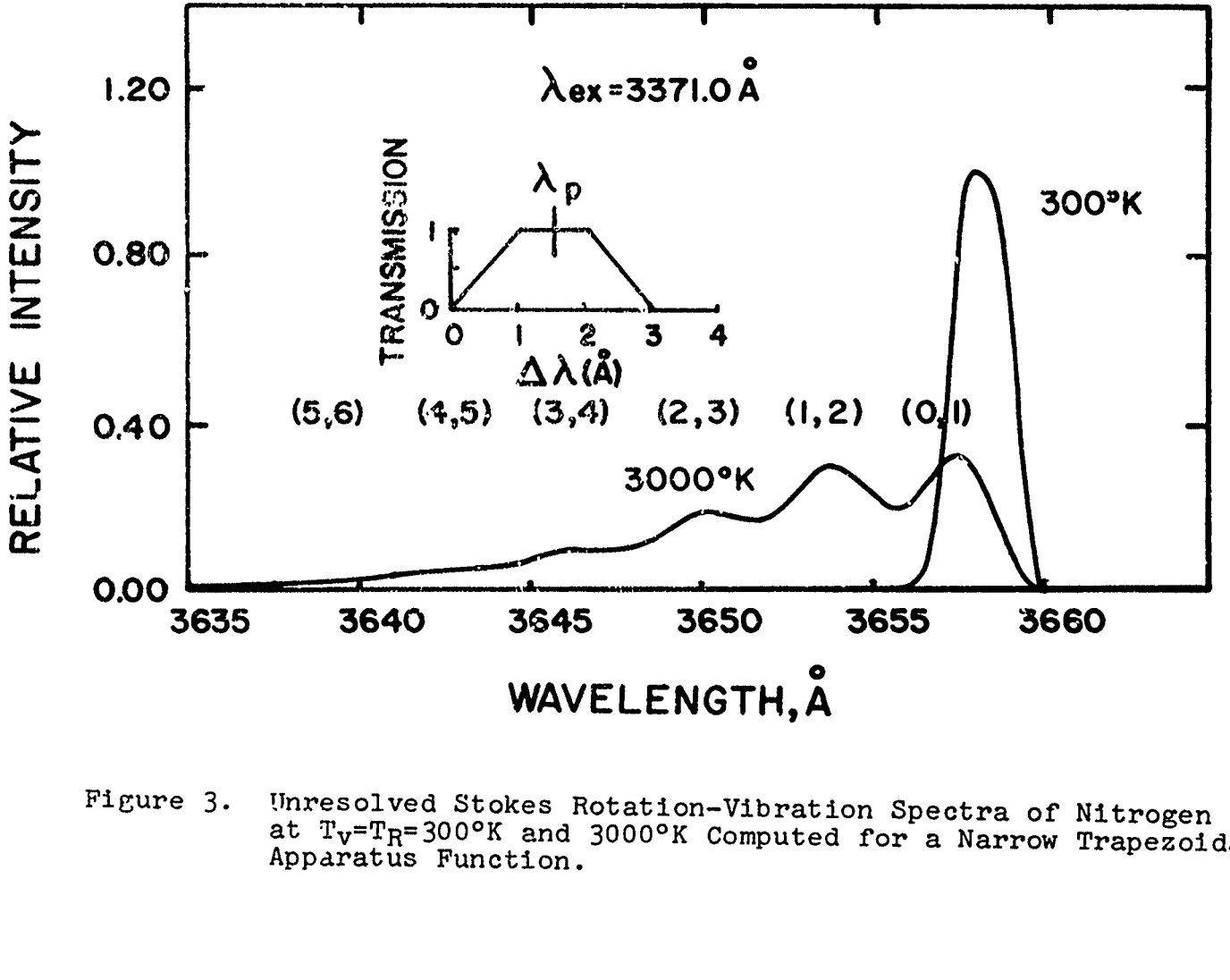

Figure 3. Unresolved Stokes Rotation-Vibration Spectra of Nitrogen at $T_V=T_R=300°K$ and 3000°K Computed for a Narrow Trapezoidal Apparatus Function.

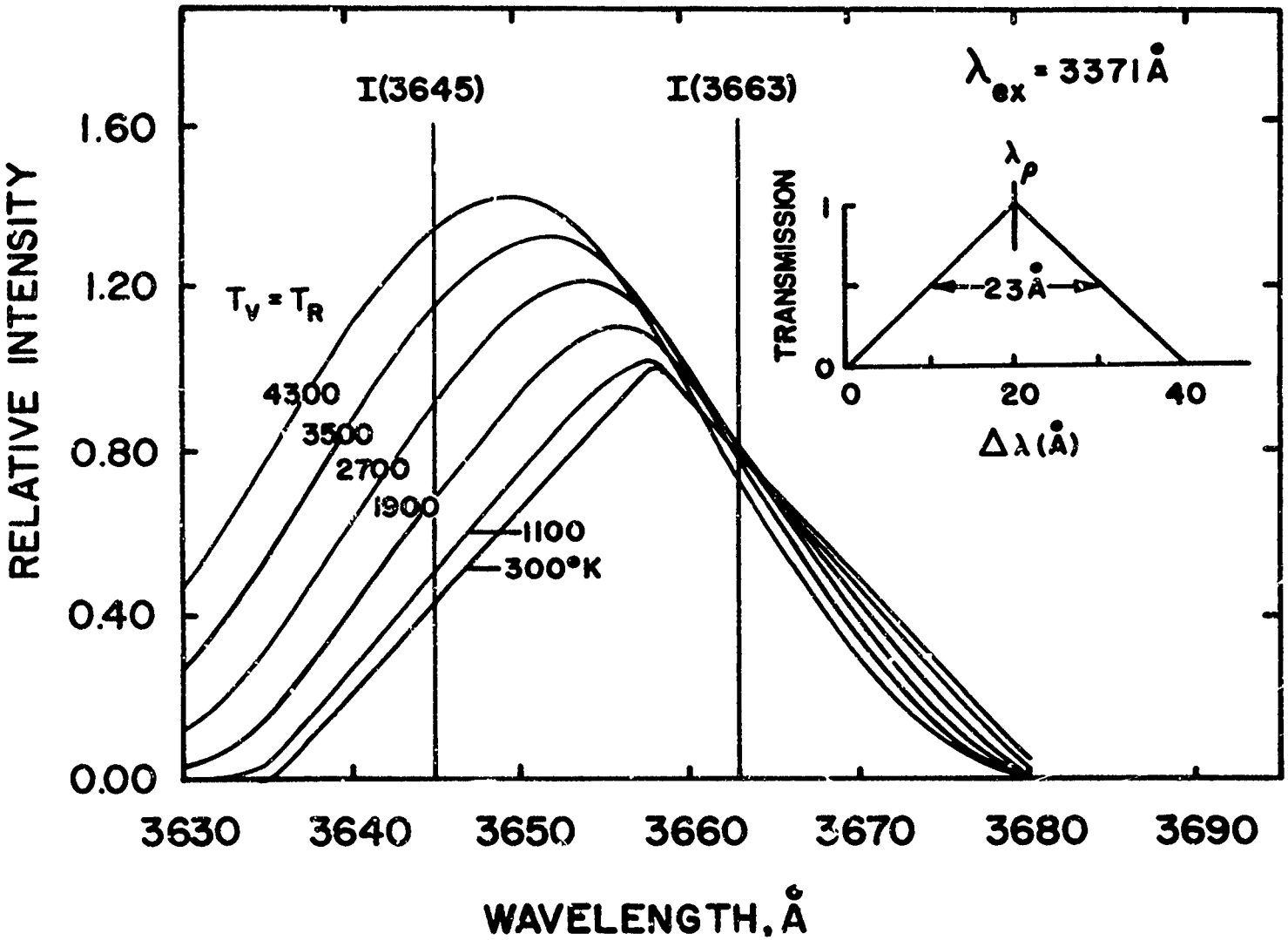

Figure 4. Unresolved Stokes Rotation-Vibration Spectra of Nitrogen at Various Temperatures Calculated Using a Broad Triangular Apparatus Function.

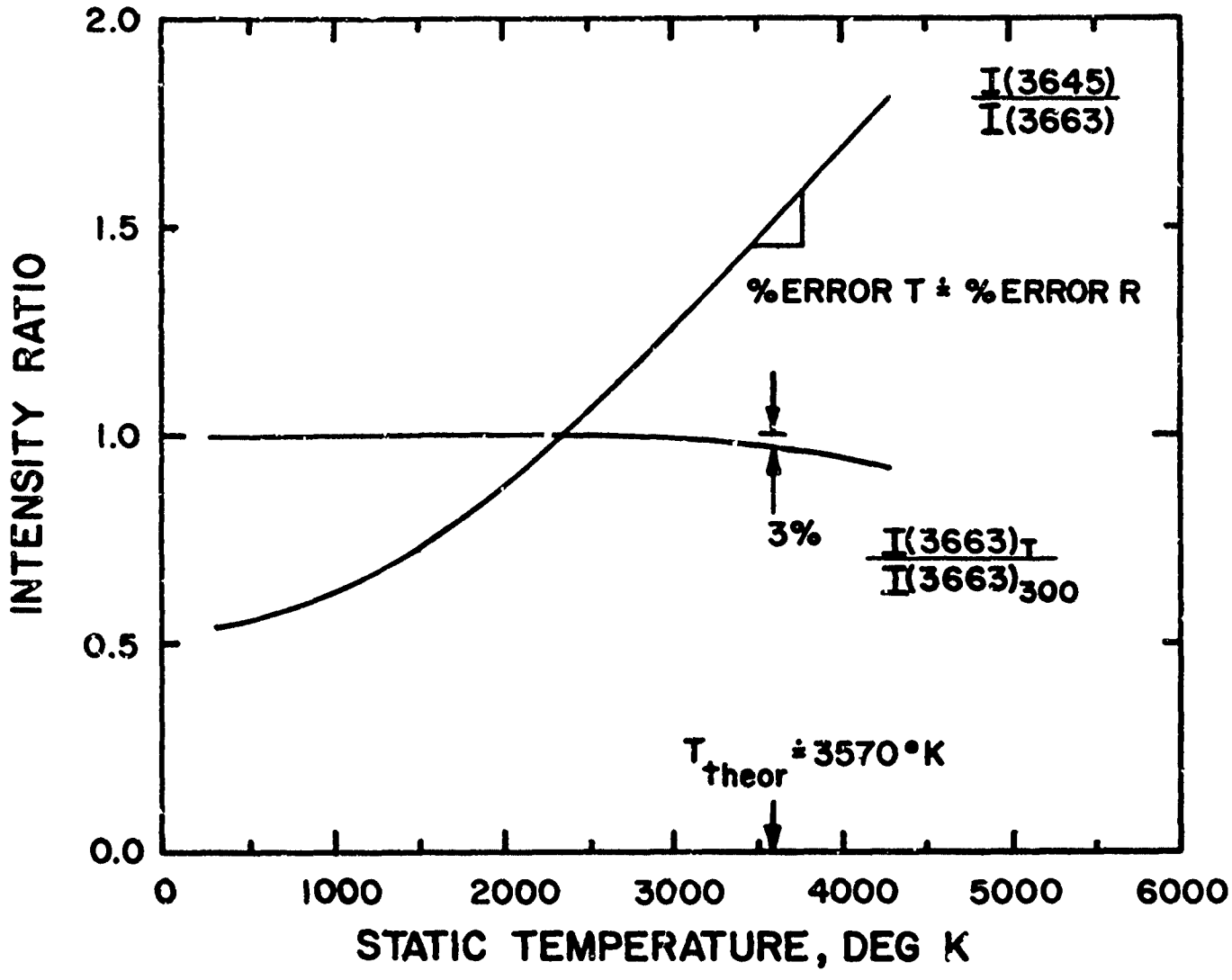

Figure 5. Nitrogen Raman Spectral Intensity Ratios Calculated as a Function of Equilibrium Temperature.

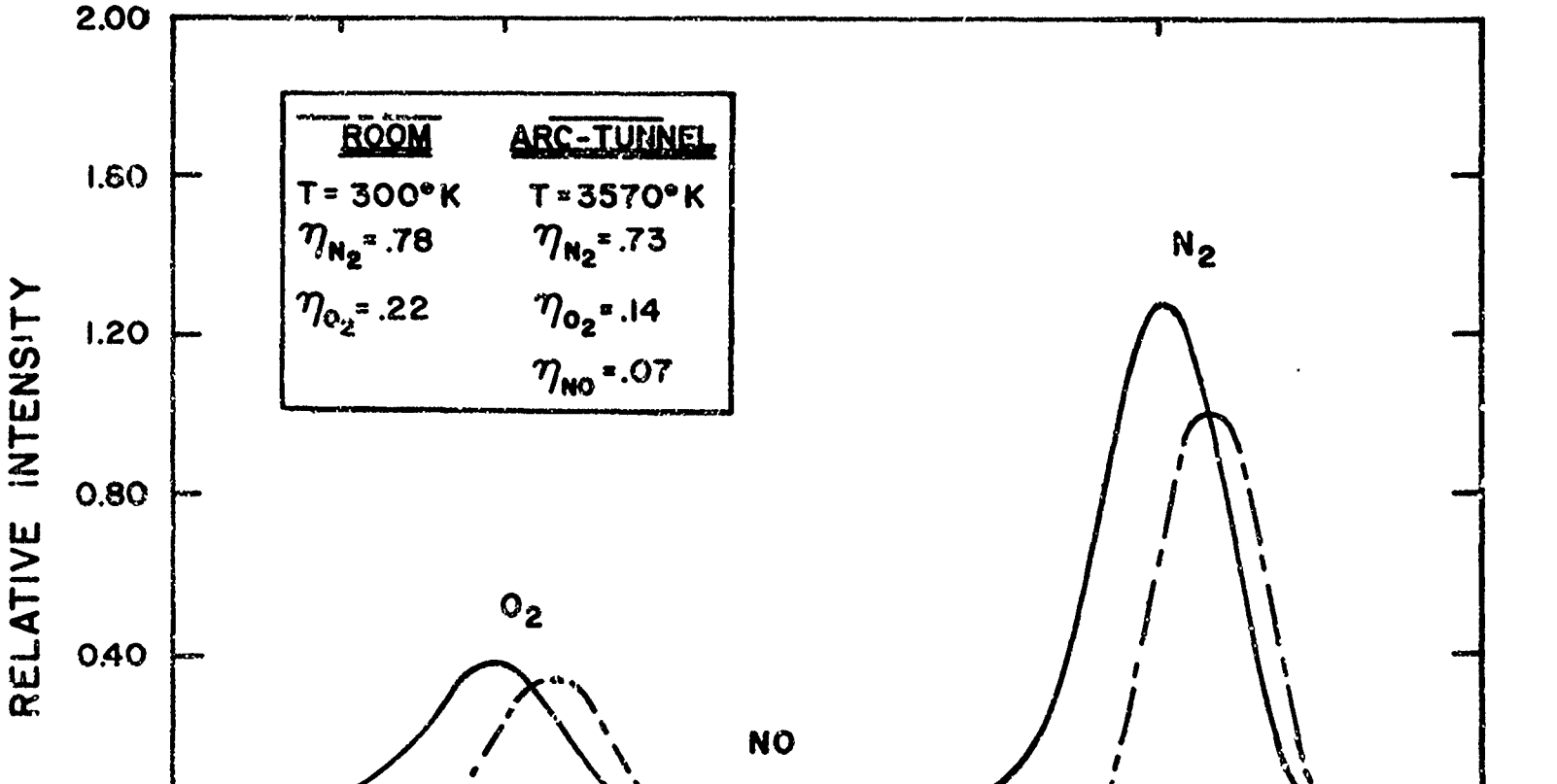

Figure 6. Raman Stokes Rotation-Vibration Spectra Computed for Air at Room and Arc-Tunnel Conditions.

Figure 7. Flow Radiation in WPAFB/FDL 50-Megawatt REMF Facility.

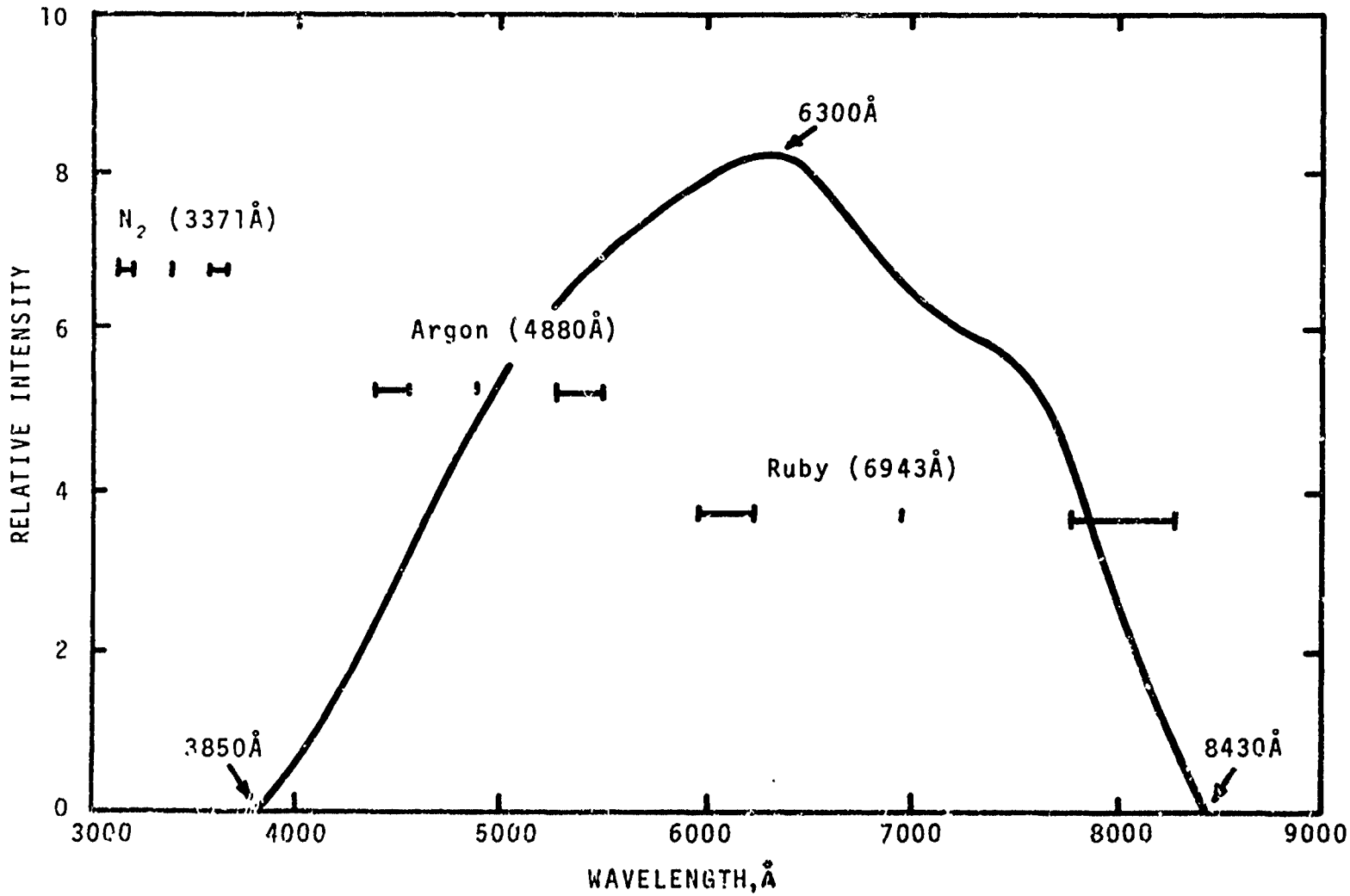

Figure 8. Measured Continum Flow Radiation Attributed to NO+O Chemiluminescence.

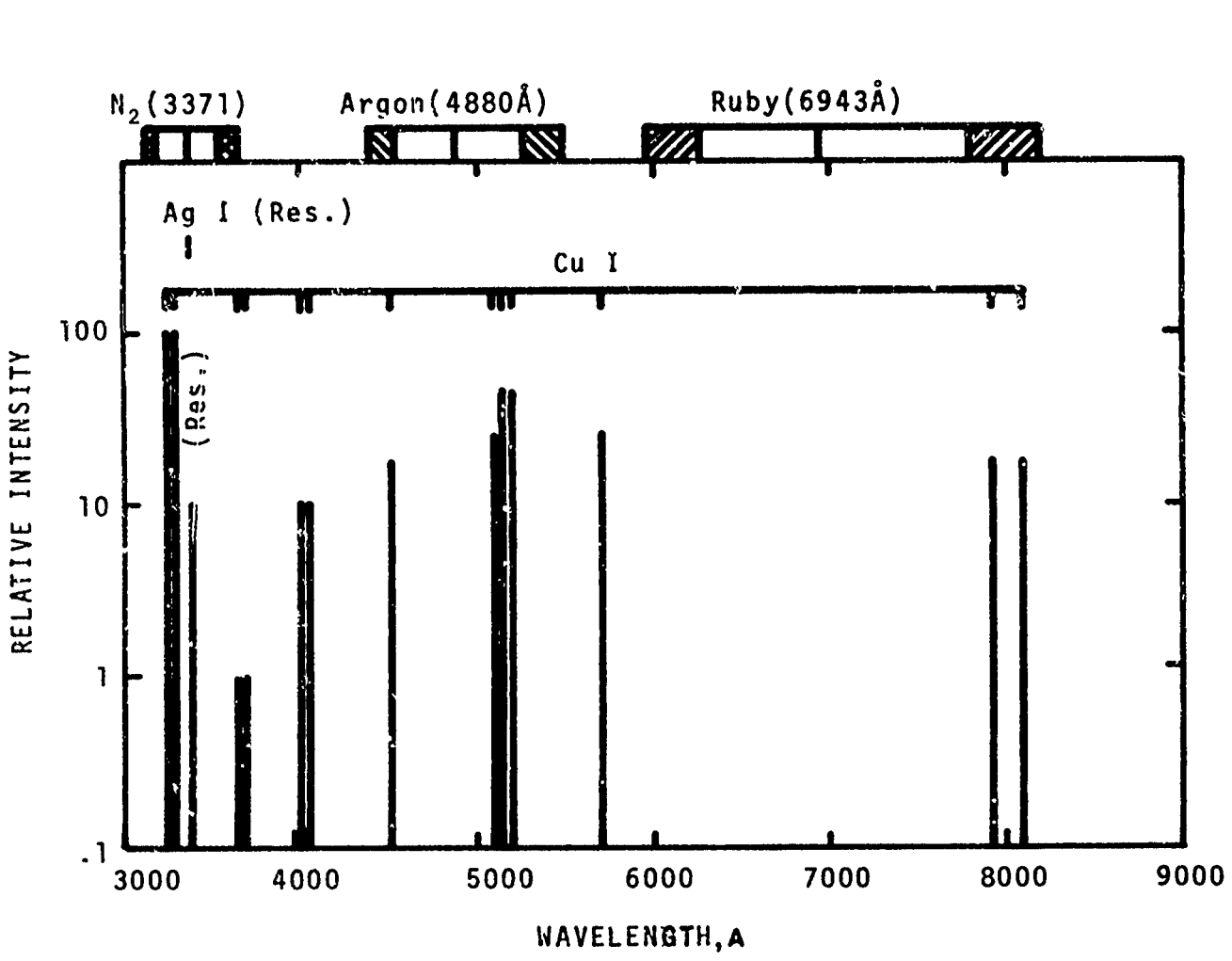

Figure 9. Estimated Atomic Line Radiation from Copper and Silver.

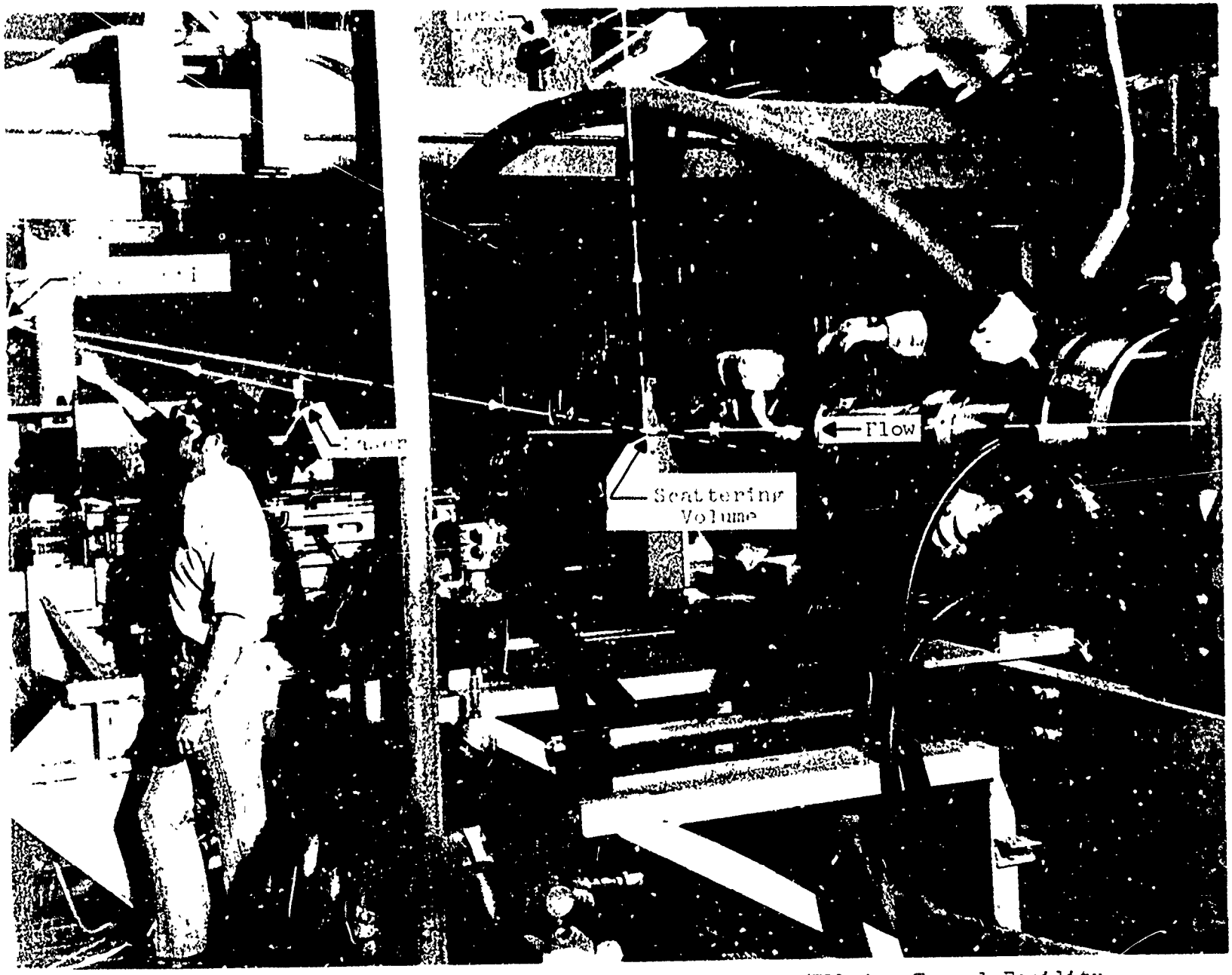

Figure 10. Raman Scattering Instrumentation in WPAFB/FDL Arc-Tunnel Facility.

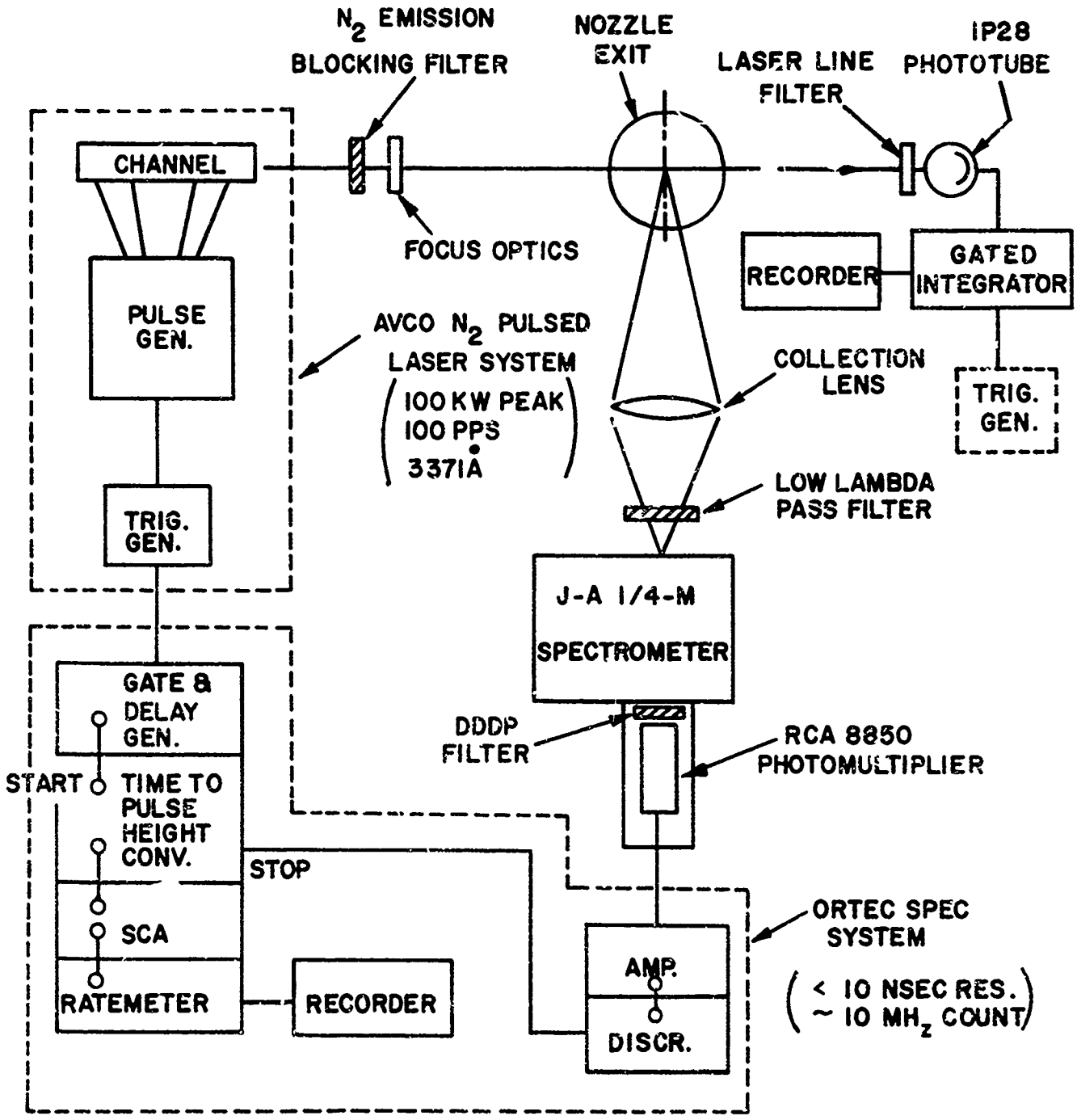

Figure 11. Block Diagram of Experimental Instrumentation Utilizing Single Photoelectron Counting (SPEC) System.

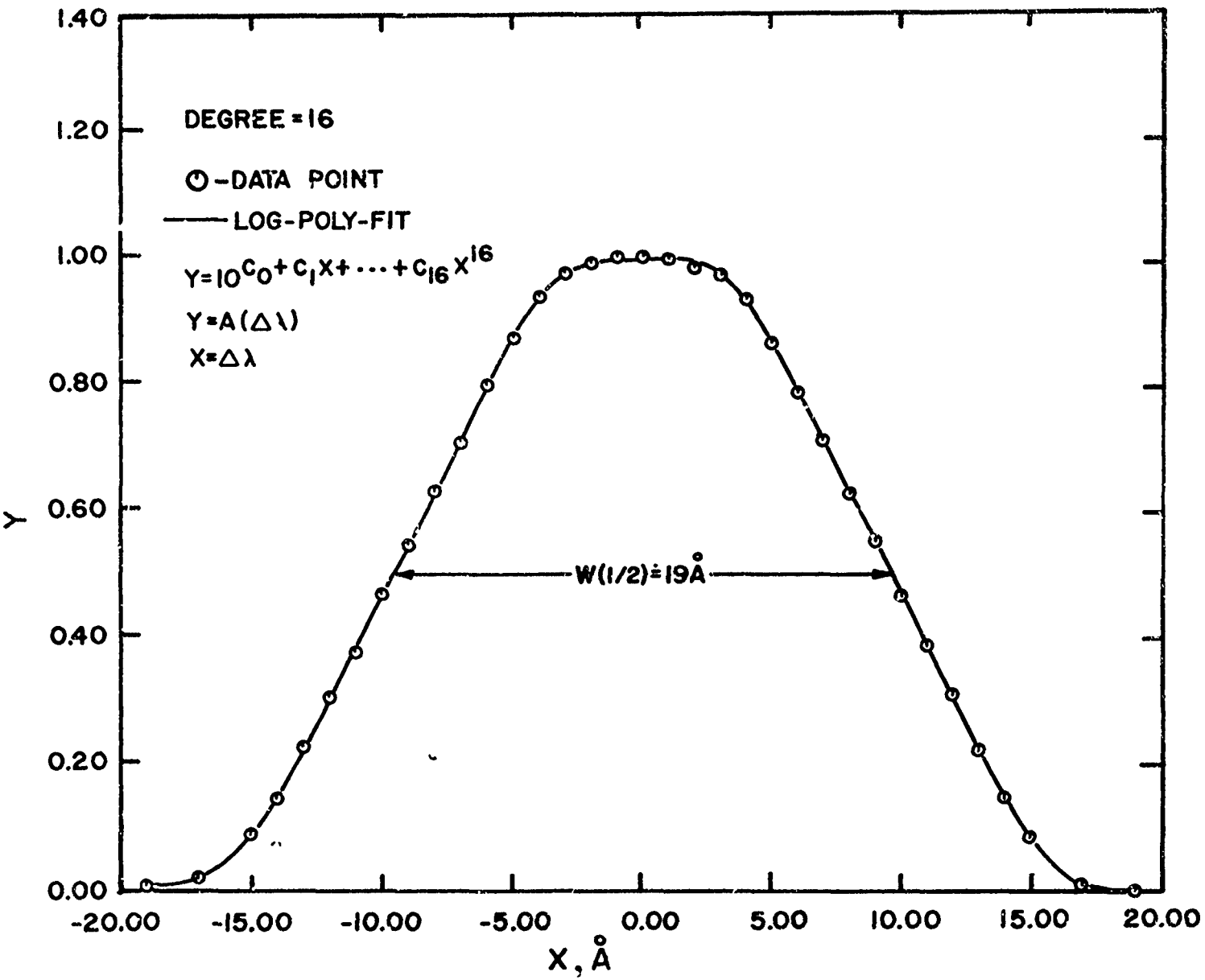

Figure 12. Log-Poly Fit of Spectrometer Apparatus Function.

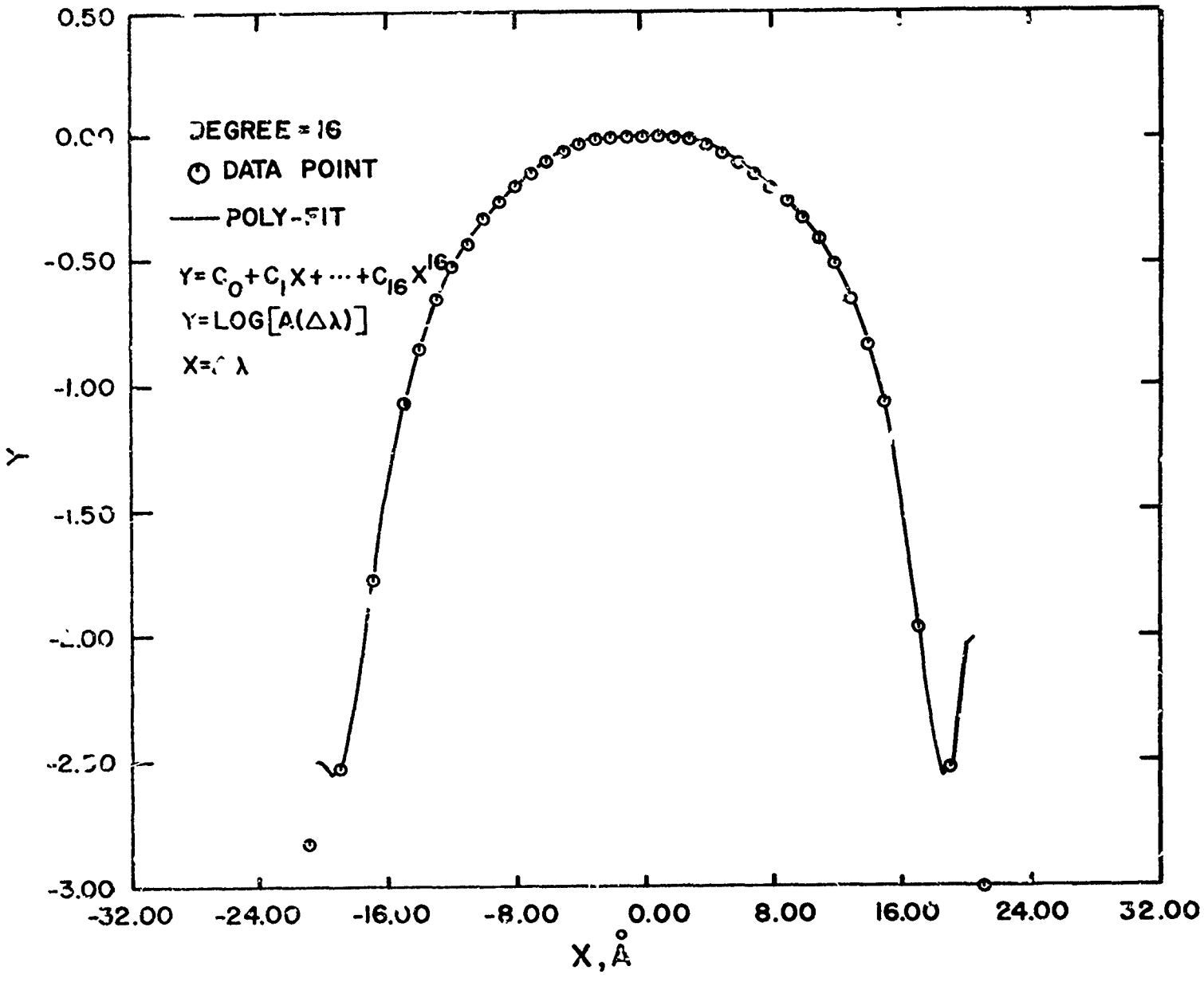

Figure 13. Polynomial Fit of Log of the Apparatus Function.

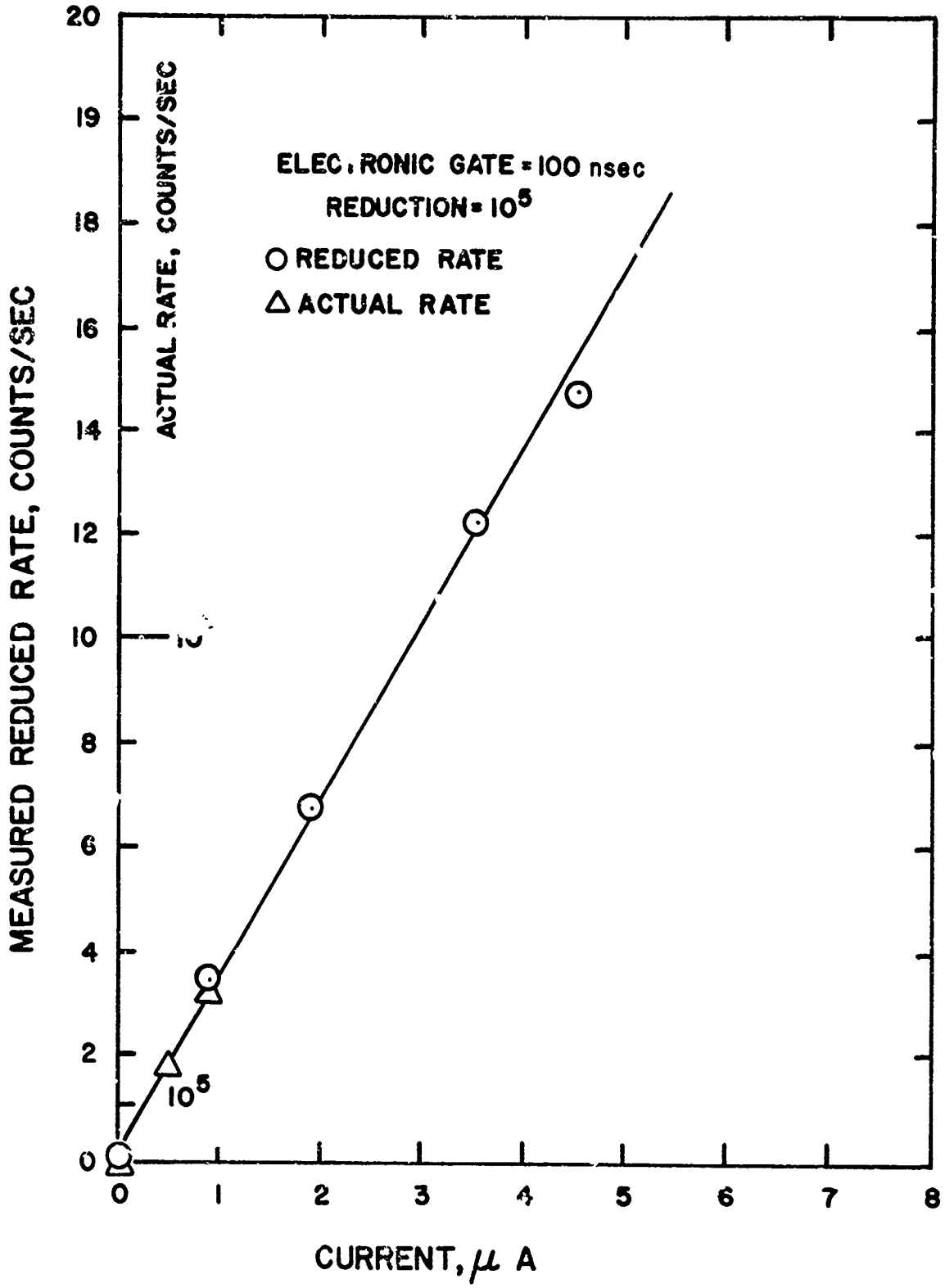

Figure 14. Linearity and Background Count Reduction Check of the SPEC System.

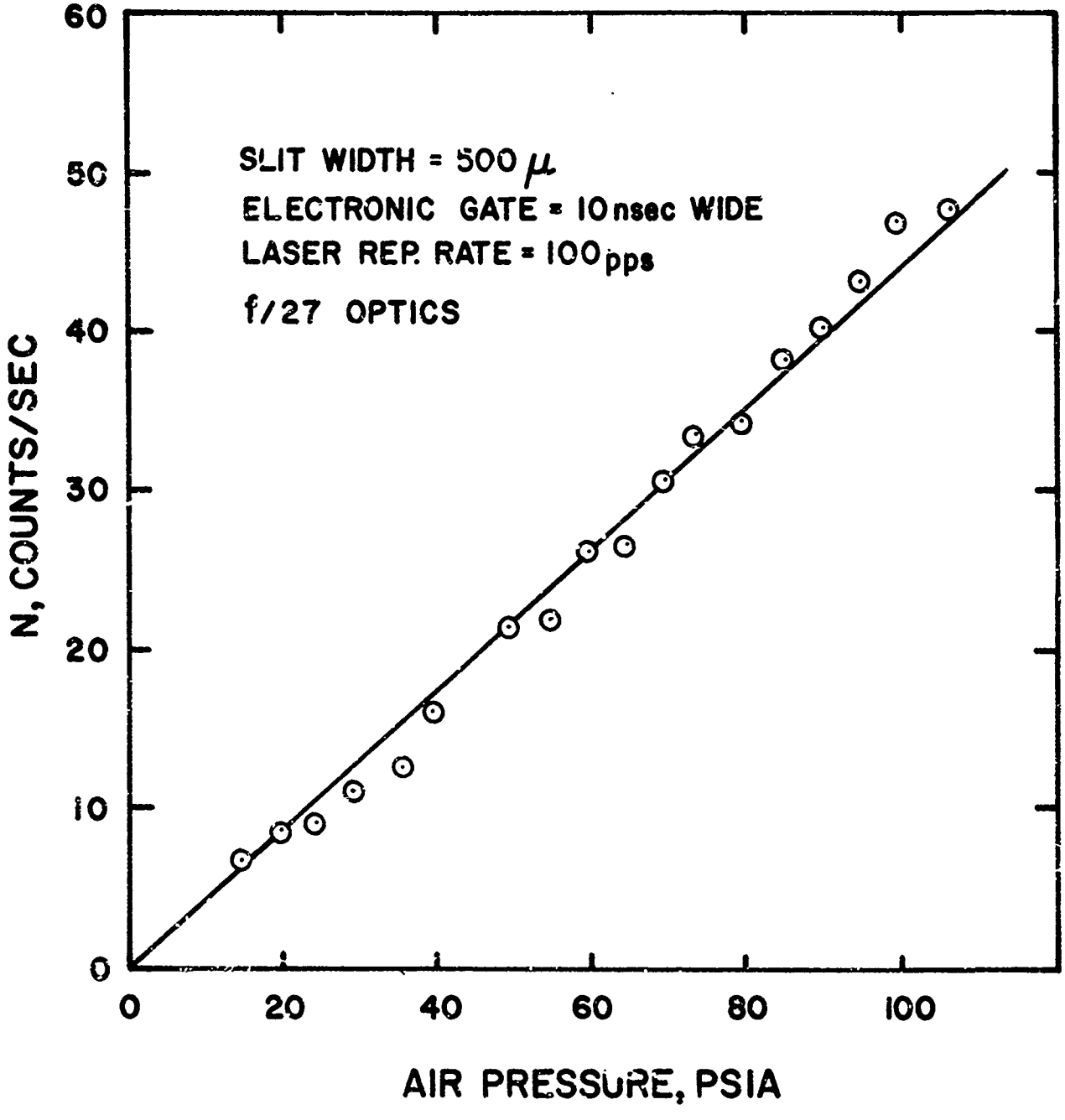

Figure 15. Nitrogen Raman Band Intensity Variation with Air Pressure in Laboratory Environment.

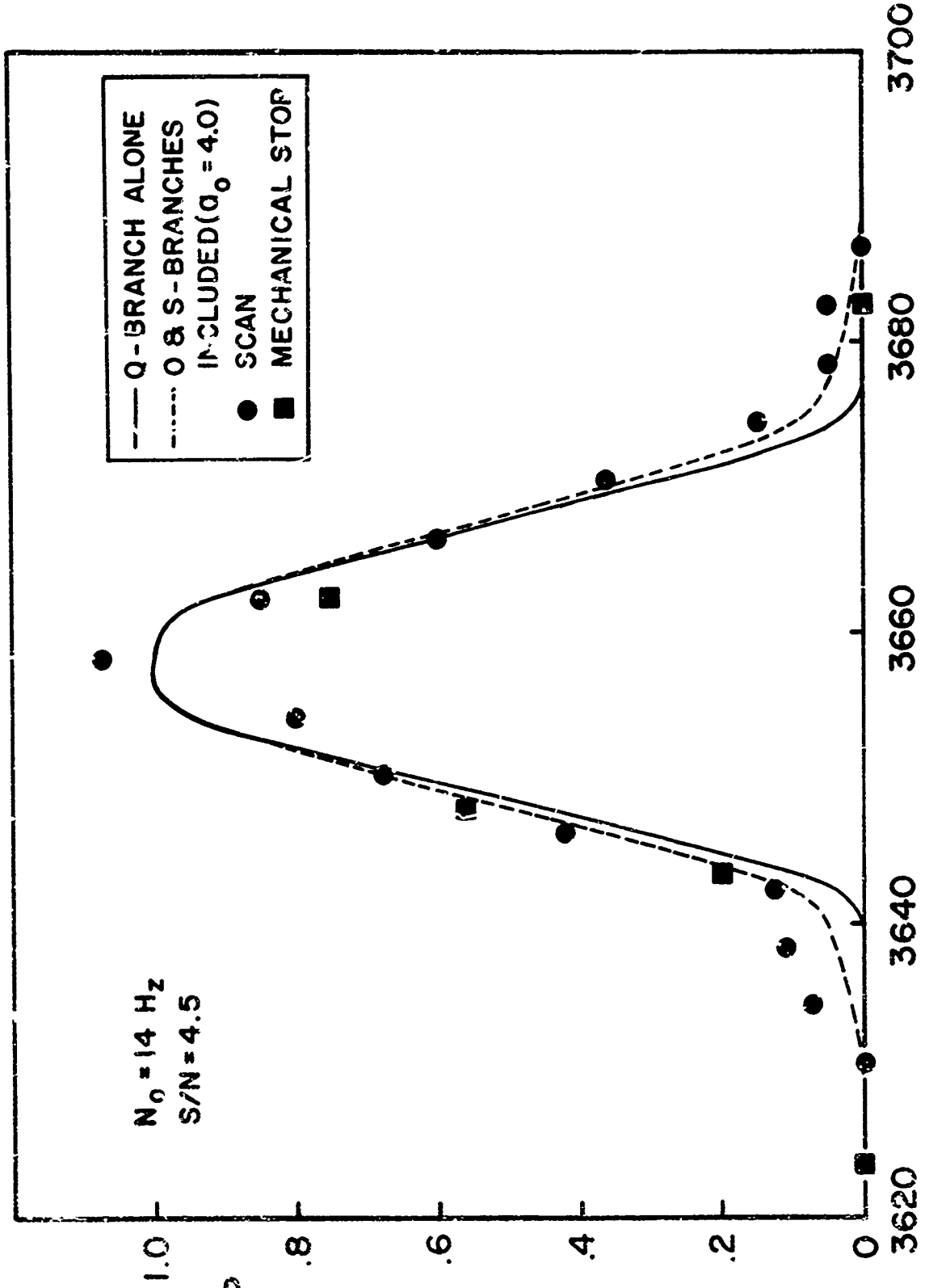

Figure 16. Nitrogen Raman Rotation-Vibration Spectrum at Room Conditions in the RENT Facility Environment.

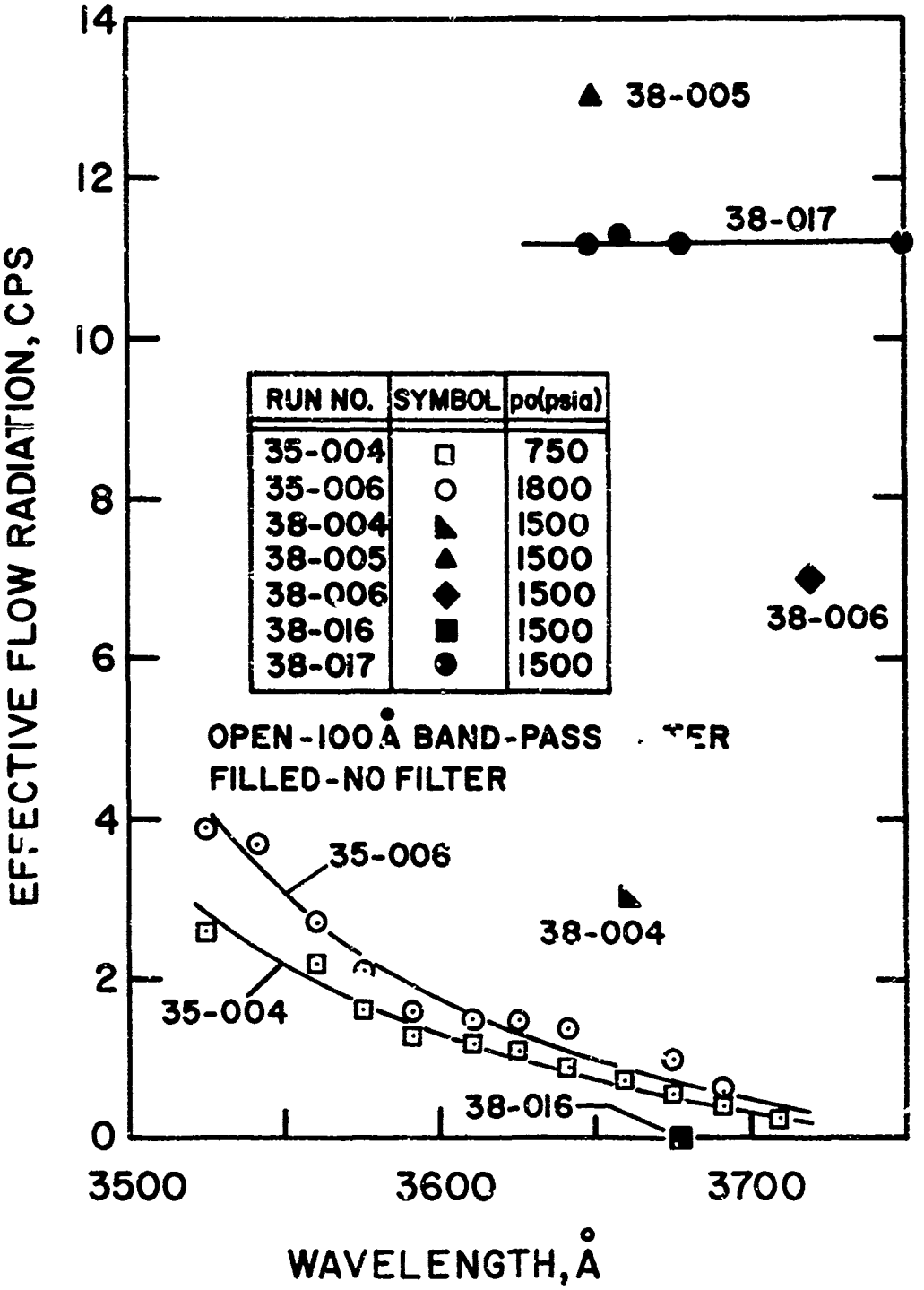

Figure 17. Effective Background Count Rate in the Raman Spectral Region During Various Arc-Tunnel Runs.

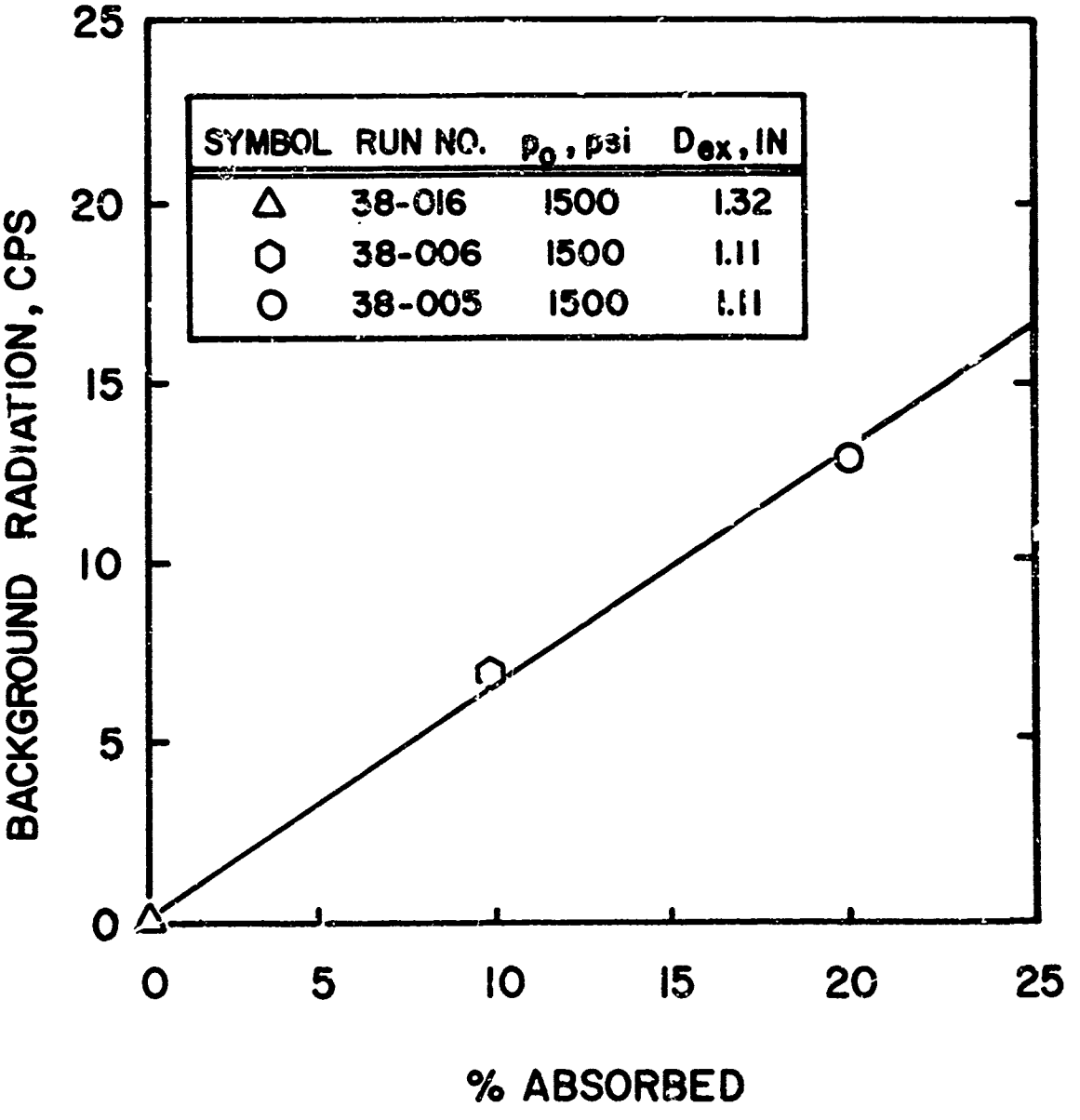

Figure 18. Laser Beam Attenuation and Flow Emission for Various Arc-Tunnel Runs.

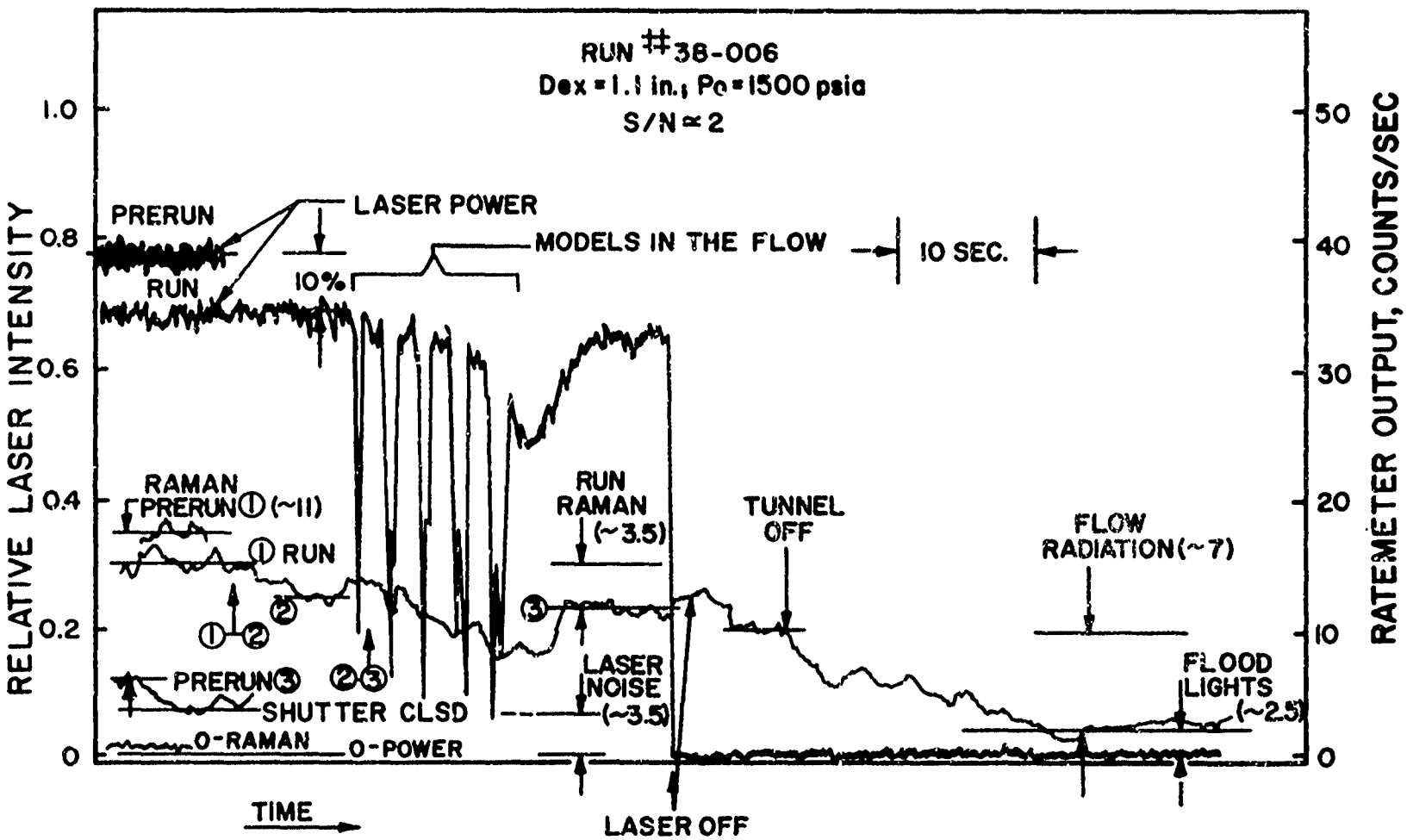

Figure 19. Test Data Record.

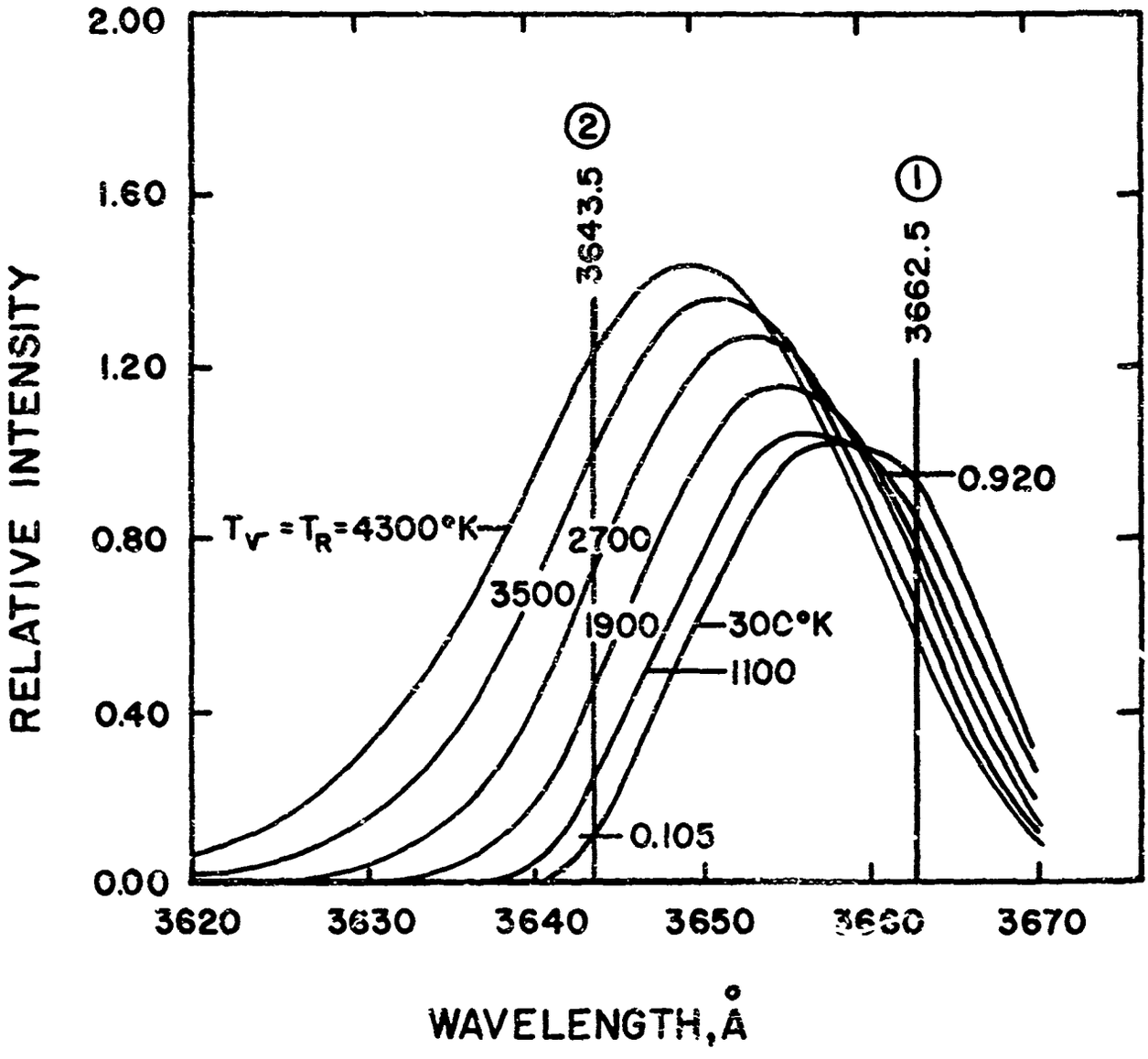

Figure 20. Calculated Nitrogen Raman Rotation-Vibration Spectral Profile at Various Temperatures Using the Measured Spectrometer Apparatus Function.

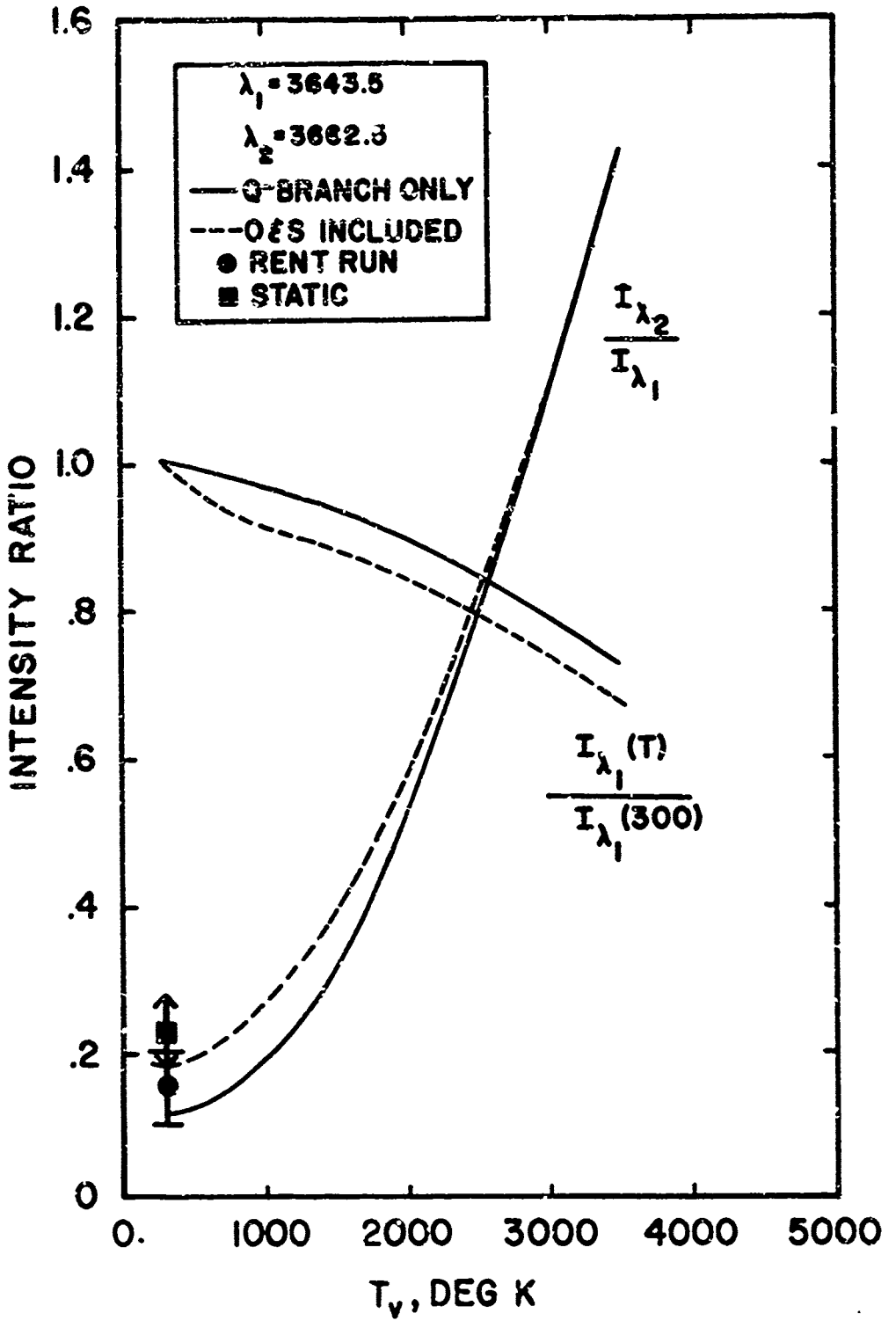

Figure 21. Raman Intensity Ratios Versus Vibrational Temperature of Nitrogen.

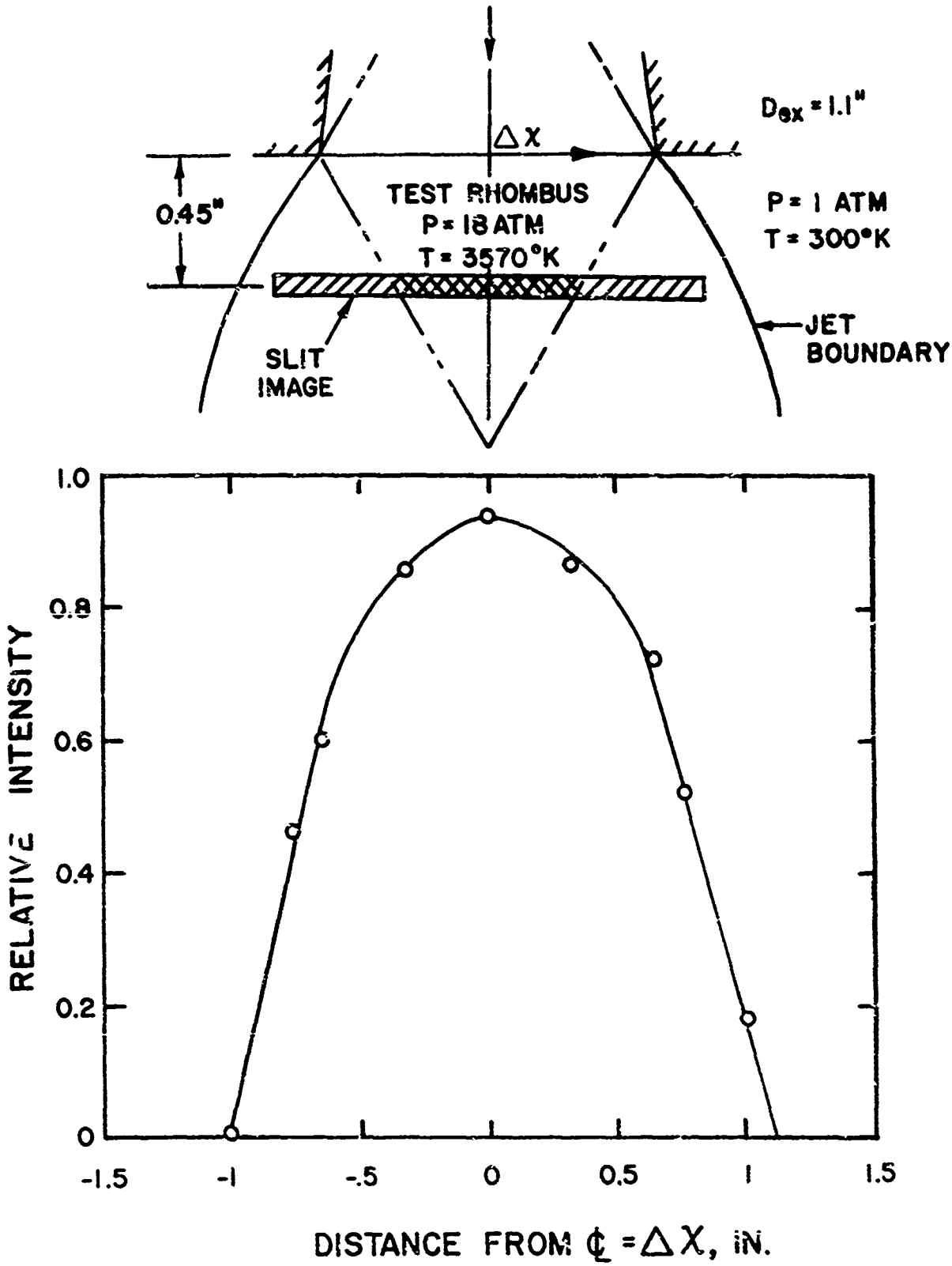

Figure 22. Spatial Resolution of Optical System.

REFERENCES

1. Rhodes, R.P., "Probing Techniques for Use in High Temperature Reacting Flows," AEDC-TR-68-44, March 1968.

2. Petrie, S.L. and Boiarski, A.A., "Electron Beam Flow Field Analyses in the AFFDL Two-Foot Electrogasdynamics Facility," AFFDL TR 71-161, December 1971.

3. Sebacher, D.I. and Duckett, R.J., "A Spectroscopic Analysis of a 1-Foot Hypersonic Arc-Tunnel Air Stream Using an Electron Beam Probe," NASA TR-R-114, 1964.

4. Mastrup, F.N., "Development of Spectroscopic and Optical Scattering Diagnostics for Nonequilibrium Reacting Gas Flows," AFFDL TR 70-17, February 1970.

5. Mastrup, F.N. and Herrett, R.H., "Optical Scattering Diagnostic Technique for Hypersonic Arc Flows," AFFDL TR 71-41, May 1971.

6. Olsen, H.N., Kelly, F.L. and Bedjai, G., "Temperature Measurements in FDL 50-Megawatt Electrogasdynamic Facility," AEDC TR 70-238, October 1970.

7. Urtz, R.P. Jr., "Plasma Specie Probe Techniques," RADC TR 66-793, February 1967.

8. Hartley, D.L., "Transient Gas Concentration Measurements Utilizing Laser Raman Spectroscopy," AIAA J 10, pp 687-689, May 1972.

9. Kellam, J.M. and Glick, M.M, "Gas Density Measurements in a Jet Using Raman Scattering," AIAA J 10, pp 1389-1391, October 1972.

10. Raman, C.V., Indian Journal Physics 2, p 387, 1928.

11. Smekel, A., "Zuschriften und Vorlaufige Mitteilungen," Naturwiss 11, p 873, September 1923.

12. Kramers, H.A. and Heisenberg, W., "Uber die Streuung von Strahlung durch Atome," Z. Physik 31, p 681, January 1924.

13. Placzek, G., "The Rayleigh and Raman Scattering," UCRL-Trans-526(1), translated from a publication of the Akademische Verlagsgesellscaft G.M.B.H., Leipzig, 1934.

14. Herzberg, G., Spectra of Diatomic Molecules, D. van Nostrand Company, Inc., New York, pp 552-561, 1950.

15. Beachler, J.C., "Operating Characteristics of the Air Force Flight Dynamics Laboratory Reentry Nose Tip (RENT) Facility," Paper No. 55, 5th Space Simulation Conference, Gaithersburg, Maryland (NBS Special Pub. No. 336), 1970.

16. Strong, J., Concepts of Classical Optics, W.H. Freeman and Company, San Francisco and London, pp 344-350, 1958.

17. Leonard, D.A., "Feasibility Study of Remote Monitoring of Gas Pollutant Emissions by Raman Spectroscopy," Avco Research Report 362, December 1970.

18. Ortec Application Note AN35, "The Single-Photon Technique for Measuring Light Intensity and Decay Characteristics," ORTEC Incorporated, 1971.

19. Penny, C.M., Goldman, L.M. and Lapp, M., "Raman Scattering Cross Sections," Nature Physical Science 235, pp 110-112, February 1972.

20. Lawrence, L.R. Jr., Walterick, R.E., Weeks, T.M. and Doyle, J.P. Jr., "Total Enthalpy Measurements from Blunt-Body Gas Cap Emission in Arc-Heated Wind Tunnels," Paper No. 72-1021, AIAA 7th Aerodynamic Testing Conference, Palo Alto, California, September 1972.